Title

Long-term functional regeneration of radiation-damaged salivary glands through delivery of a neurogenic hydrogel

Journal

Science Advances, 8(51)

ISSN

2375-2548

Authors

Li, Jianlong
Sudiwala, Sonia
Berthoin, Lionel
et al.

Publication Date

2022-12-23

DOI

10.1126/sciadv.adc8753

Peer reviewed

CELL BIOLOGY

Long-term functional regeneration of radiation-damaged salivary glands through delivery of a neurogenic hydrogel

Jianlong Li[1]†, Sonia Sudiwala[1]†, Lionel Berthoin[1]†, Seayar Mohabbat[1], Eliza A. Gaylord[1], Hanan Sinada[1], Noel Cruz Pacheco[1], Jiun Chiun Chang[2], Oju Jeon[3], Isabelle M.A. Lombaert[4,5], Alison J. May[1]‡§, Eben Alsberg[3,6]‡, Chelsea S. Bahney[2,7]*‡, Sarah M. Knox[1]*‡

Salivary gland acinar cells are severely depleted after radiotherapy for head and neck cancer, leading to loss of saliva and extensive oro-digestive complications. With no regenerative therapies available, organ dysfunction is irreversible. Here, using the adult murine system, we demonstrate that radiation-damaged salivary glands can be functionally regenerated via sustained delivery of the neurogenic muscarinic receptor agonist cevimeline. We show that endogenous gland repair coincides with increased nerve activity and acinar cell division that is limited to the first week after radiation, with extensive acinar cell degeneration, dysfunction, and cholinergic denervation occurring thereafter. However, we found that mimicking cholinergic muscarinic input via sustained local delivery of a cevimeline–alginate hydrogel was sufficient to regenerate innervated acini and retain physiological saliva secretion at nonirradiated levels over the long term (>3 months). Thus, we reveal a previously unknown regenerative approach for restoring epithelial organ structure and function that has extensive implications for human patients.

INTRODUCTION

Despite substantial improvements in the targeted delivery of ionizing radiation (IR) for the treatment of tumors of the head and neck, numerous neighboring tissues and organs, including the oral mucosa (*1*), mandible/maxilla bone and dentition (*2*), blood vessels (*3*), masticatory musculature and apparatus (*4*), and salivary glands (*5*), are inadvertently damaged by off-target effects. With IR being the primary treatment option for the elimination of head and neck cancers [67,000 per year in the United States (*6*)], salivary glands represent one of the organ systems routinely injured, often resulting in permanent hyposalivation and related dry mouth condition xerostomia (*7*). As saliva plays a multitude of roles in maintaining oral and gastrointestinal health, pathological injury to these glands causes a diverse array of complications, including poor digestion, accelerated dental caries, periodontal disease, esophageal infections, and gastroesophageal reflux disease (*7*). With no curative therapies available, these outcomes are irreversible.

The off-target effects of radiotherapy occur across time, with transient acute effects occurring within days to weeks of treatment and intermediate-to-late effects being initiated months to years later, resulting in eventual (and irreversible) tissue dysfunction and degeneration (*8*). While the time frame of structural damage to each tissue depends on its functional tolerance and volume effect, in general, acute effects are due to cell death, and intermediate-to-late effects are primarily characterized by damage to vascular, stromal, and neuronal cells. The resulting chronic effects are then defined by complex damage that is too severe to repair (*8*, *9*). With regard to salivary glands, irradiation affects multiple cell types and structures, including acinar cells, myoepithelial cells, duct cells, nerves, blood vessels, and supporting stromal tissue, which contribute to saliva production (*3*, *9*–*12*). However, loss of saliva production after IR therapy has been primarily attributed to the destruction of a major secretory cell type, the acinar cell (*13*, *14*). Both serous and mucous acini belonging to the three major salivary glands (i.e., parotid, submandibular, and sublingual) secrete a fluid containing water, electrolytes, mucus, and proteins, e.g., enzymes and immunoglobulins, into the ductal system for deposition within the oral cavity. Numerous studies have demonstrated these cells to be gradually destroyed after IR exposure, with rodents and humans exhibiting extensive loss of serous acinar cells within 2 to 3 months (*14*, *15*). While fractionation models in rodents may more directly recapitulate the clinical situation and influence acute responses, single-dose studies certainly also provide consistent loss of salivary gland function and serve as equally valuable research models to study radiation-induced effects (*16*, *17*). Unfortunately, no regenerative treatments are currently available to promote the repopulation of acinar cells and repair organ function post-IR. Furthermore, current palliative treatment options, such as salivary stimulants, topical agents, saliva substitutes, systemic sialagogues, and mouth rinses, do not recapitulate the multifunctional roles of saliva, thus resulting in pronounced patient morbidity over their lifetime (*18*).

[1]Department of Cell and Tissue Biology, University of California, San Francisco, San Francisco, CA, USA. [2]Orthopedic Trauma Institute, University of California, San Francisco, San Francisco, CA, USA. [3]Department of Biomedical Engineering, University of Illinois, Chicago, Chicago, IL, USA. [4]Biointerfaces Institute, University of Michigan, Ann Arbor, MI, USA. [5]Department of Biologic and Materials Sciences, University of Michigan School of Dentistry, Ann Arbor, MI, USA. [6]Departments of Orthopedics, Pharmacology and Regenerative Medicine, and Mechanical and Industrial Engineering, University of Illinois, Chicago, Chicago, IL, USA. [7]Center for Regenerative Sports Medicine, Steadman Philippon Research Institute, Vail, CO, USA.
*Corresponding author. Email: sarah.knox@ucsf.edu (S.M.K.); cbahney@sprivail.org (C.S.B.)
†These authors contributed equally to this work.
‡These authors contributed equally to this work as co–senior authors.
§Present address: Departments of Cell, Developmental and Regenerative Biology and Otolaryngology, Icahn School of Medicine at Mount Sinai, New York, NY, USA.

In addition to destroying salivary gland acinar cells, IR therapy has also been shown to deplete the parasympathetic nerve supply (*10*). Parasympathetic nerves are an essential driver of acinar cell function, maintenance, and repair, with studies over the past 60+ years showing a clear requirement for these nerves in glandular function and homeostasis (*10*, *19*, *20*), with nerve damage resulting in glandular atrophy (*19*, *20*) and reinnervation promoting tissue regeneration (*10*, *21*, *22*). Multiple studies have further revealed that the positive feedback loop between parasympathetic nerves and acinar cells is crucial to homeostasis, and that loss in either signaling loop, e.g., nerve acetylcholine-muscarinic signaling to acini or acinar neurotrophic signaling to nerves, results in tissue degeneration (*23*). More specifically, in vivo studies indicate that stimulation of muscarinic receptors is necessary to promote the division of acinar ($SOX2^+$) progenitors and their transit-amplifying ($SOX2^-$) progeny (*10*), supporting a role for this pathway in acinar cell replenishment. Furthermore, application of a synthetic muscarinic agonist (e.g., carbachol) to ex vivo cultures of irradiated adult tissue is sufficient to repopulate acinar cells at least during the first 48 hours following IR treatment (*10*). However, it remains unknown whether acinar cells retain their ability to undergo cell division in response to muscarinic activation (i.e., beyond 48 hours post-IR) and whether reestablishing the muscarinic pathway post-IR can regenerate functional acini. Moreover, whether parasympathetic nerve–acinar cell communication can be restored in the irradiated tissue to mediate long-term organ function and homeostasis has not been determined.

Through a series of in vivo studies, we show that local delivery of the muscarinic receptor (CHRM1 and CHRM3) agonist, cevimeline (CV), encapsulated in an alginate hydrogel (ALG) to irradiated salivary glands is highly efficacious in maintaining saliva secretion and glandular function over an extended time period that is typically associated with glandular degeneration. We demonstrate that radiation-induced loss of acinar cell proliferation and parasympathetic innervation is rescued by muscarinic receptor activation, thereby ensuring the preservation of the acinar cell pool and a functional nerve supply required for homeostatic and secretory processes. Thus, we provide a previously unknown therapeutic approach for the long-term restoration of salivary gland function after radiation therapy.

RESULTS

Acinar cells undergo a time-limited regenerative response 1 week following radiation exposure that correlates with an increase in neuronal-related genes

We previously demonstrated that mucous acinar cells in the murine salivary (sublingual) gland are actively replaced by $SOX2^+$ progenitor cells during the first 2 weeks following IR treatment (*10*). However, whether acinar cells continuously repopulate the organ during this time frame, and whether changes in nerve-derived muscarinic input are involved, remains to be determined. Thus, we first questioned the timing of endogenous regenerative events in response to a single 10-Gy dose of IR by sequencing the transcriptomes of glands from adult (6 to 7 weeks) mice at 7 and 14 days post-IR and comparing to non-IR controls (Fig. 1A and fig. S1A). Differential gene expression analysis [DESeq2 (*24*); $P_{adj} < 0.1$; 1.5-fold change cutoff] revealed extensive alterations in gene expression at the 7-day post-IR time point compared to non-IR controls, with 1354 genes being up-regulated and 1122 down-regulated (Fig. 1B, fig. S1B, and data S1). Gene ontology (GO) enrichment analysis of the significantly changed genes using g:Profiler (*25*) identified a marked increase in genes associated with cell division (Fig. 1, A and B). These included positive regulators of cell cycle progression (e.g., *Cdk1*, *Bub1*, *Ccnd1*, and *Plk1*; $P < 0.01$), with particular enrichment for genes associated with mitotic events, such as spindle assembly, chromatid segregation (e.g., *Tpx2*, *Nek2*, *Kif23*, and *Birc5*; $P < 0.01$), and cytokinesis (e.g., *Cep55* and *Ndc80*; $P < 0.001$) (Fig. 1A). The down-regulated genes were primarily involved in protein synthesis and mitochondrial oxidative phosphorylation (fig. S1B), suggesting that a reduction in secretory processes occurs simultaneously with an increase in proliferation over the first 7 days.

To determine changes in gene expression across time, we next measured alterations in gene transcript levels at 14 days post-IR compared to the 7-day time point and found 323 genes to be up-regulated and 324 down-regulated (data S2). As shown in Fig. 1, the most significant increase was associated with the immune system (128 genes), with extensive up-regulation of genes/pathways involved in the innate immune response that is indicative of tissue injury, including the master transcription factors *Irf5* ($P < 0.05$) (*26*) and *Irf7* ($P < 0.01$) (*27*) and markers of systemically recruited monocytes (e.g., *Ccr2* and *Lyz2*; $P < 0.01$) (Fig. 1A) (*28*). Together with previous findings in irradiated submandibular salivary glands showing that edema or immune cell infiltrate does not occur during the first 10 days following IR (*29*), this outcome suggests that immune cell recruitment occurs between 10 and 14 days post-IR. The largest cohort of down-regulated genes at 14 days (101 genes) was associated with the cell cycle (Fig. 1, A and B), with many of the same genes that had increased at 7 days post-IR, including *Bub1*, *Ccnd1*, *Plk1*, *Tpx2*, *Kif23*, *Birc5*, and *Ndc80* ($P < 0.05$), returning to non-IR levels. In addition to the decrease in genes involved in mitosis, those involved in cell cycle progression were also down-regulated (e.g., *Rb1*, *Usp2*, *Cdk1*, *Ccne1*, and *Ccnb1*; $P < 0.05$), an outcome suggestive of cell cycle exit by 14 days post-IR (fig. S1B). Last, we determined whether the 14-day post-IR tissue was returning to the non-IR state by comparing it to non-IR controls. In contrast to 7-day post-IR glands, the number of genes differentially expressed at 14 days was low, with only 308 genes being significantly up-regulated and 121 down-regulated (fig. S1C and data S3). Analysis of GO terms revealed an up-regulation of genes involved in immune response, while only a few genes associated with responses to endoplasmic reticulum stress and negative regulation of cellular metabolisms were down-regulated. Together, these results indicate that salivary glands at 7 days post-IR are in a phase of increased cell turnover but that, by 14 days post-IR, cell proliferation is reduced to basal levels while there is an increasing tissue immune response.

Next, we performed immunofluorescent analysis to confirm changes in cell turnover and identify the proliferating cell type(s) during the 2-week time period post-IR. First, epithelial cell proliferation was quantified by immunostaining tissue for phosphohistone H3 (pHH3), a marker of the M phase of the cell cycle (*30*), and the acinar cell marker Na-K-Cl cotransporter (NKCC1). In line with the abundance of cell cycle–related genes, glands at 7 days post-IR exhibited an 81% increase in $pHH3^+$ mitotic cells, restricted to the acinar cell population, compared to the non-IR controls ($P < 0.01$; Fig. 1C and fig. S1D). Consistent with the

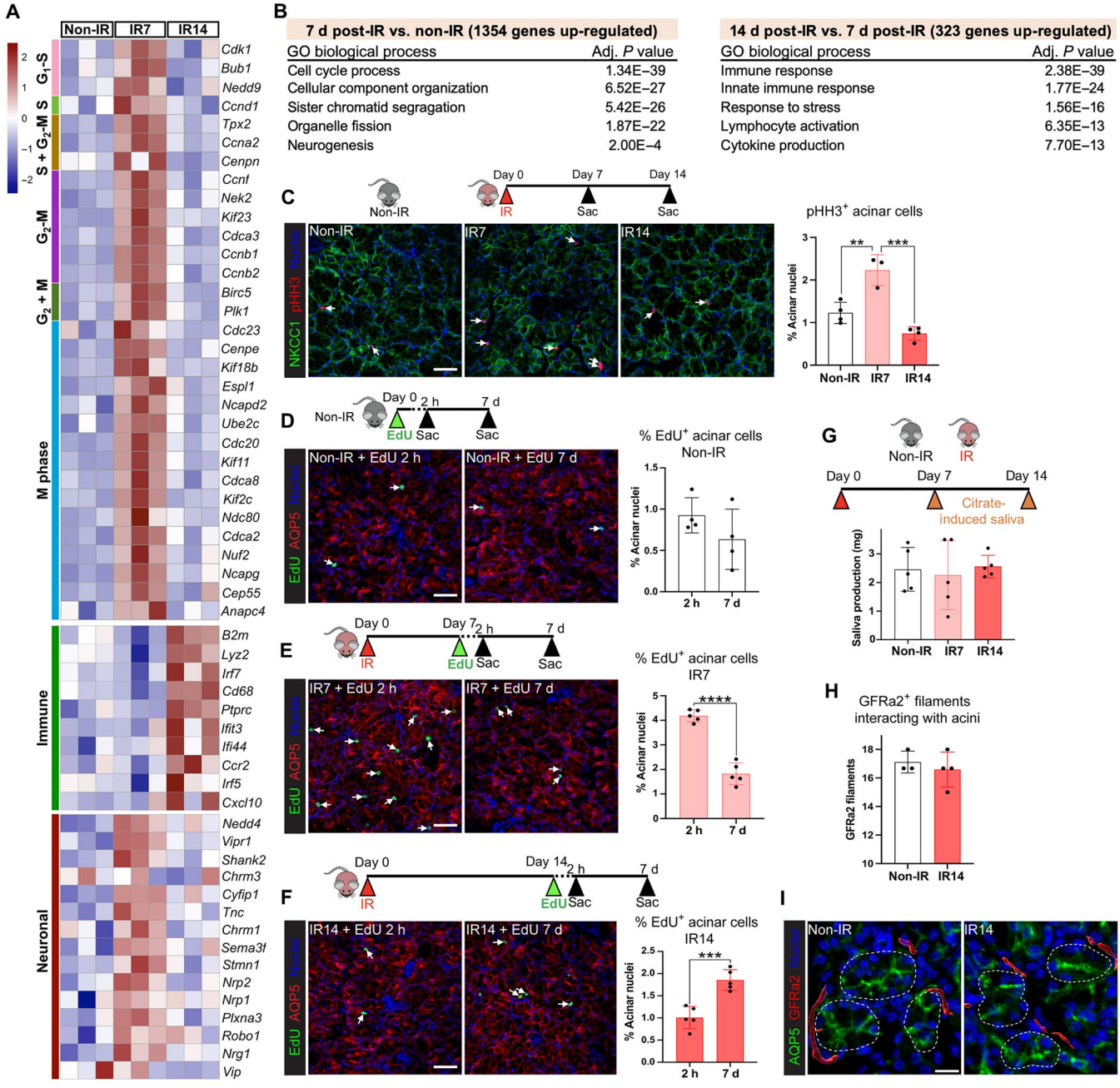

Fig. 1. Acinar cells undergo a time-limited regenerative response 1 week following radiation exposure that correlates with increased neuronal activity. (**A**) Heatmap showing mitotic, immune, and neuronal gene expression in sublingual glands at 7 or 14 days post-IR, compared to non-IR controls, $n = 3$ mice per group. (**B**) GO analysis of significantly up-regulated genes (fold change > 1.5, $P < 0.05$). (**C**) Sublingual glands from non-IR and 7- and 14-day post-IR mice immunostained for pHH3 (red), NKCC1 (green), and nuclei (blue). Arrows highlight proliferating acinar cells. pHH3$^+$ acinar cells were quantified and expressed as a percentage of the total acinar cells (graph). (**D** to **F**) Immunofluorescent detection of EdU$^+$ cells (green) in sublingual glands at 2 hours and 7 days following a single injection of EdU into non-IR mice (D) and mice at 7 days (E) and 14 days (F) post-IR. Arrows highlight proliferating acinar cells. EdU$^+$AQP5$^+$ cells were quantified and expressed as a percentage of the total acinar cells (graphs). (**G**) Citrate-induced saliva collection at 7 and 14 days post-IR and in non-IR control. (**H** and **I**) Quantification (H) of parasympathetic nerves (GFRa2, red) innervating acini (AQP5, green) in sublingual glands at 14 days post-IR versus non-IR control. Nuclei, blue. Scale bars, 40 μm (C to F) and 15 μm (I). Each dot in the bar graph represents a biological replicate. Data are expressed as means ± SD. *$P < 0.05$; **$P < 0.01$; ***$P < 0.001$; ****$P < 0.0001$; graphs (D) to (F) and H): an unpaired two-tailed t test for two-group comparisons. Graphs (C) and (G): a one-way ANOVA followed by a Dunnett's test for multiple comparisons.

transcriptomic analysis, acinar cell proliferation at 14 days post-IR was significantly reduced compared to that at 7 days (a 67% reduction; $P < 0.001$; Fig. 1C and fig. S1D) but was not significantly different from that of non-IR controls (Fig. 1C and fig. S1D).

To verify that acinar cells were undergoing cell turnover, we performed a pulse-chase assay in which EdU (5-ethynyl-2′-deoxyuridine) was systemically injected into non-IR or irradiated mice at 7 or 14 days post-IR. The number of EdU^+ acinar cells (as a percentage of the total acinar cells) was then quantified after a 2-hour or 7-day chase at each of these time points, e.g., day 7 + 2 hours or day 7 + 7 days. Consistent with previous studies (*31*), acinar cell turnover under non-IR (homeostatic) conditions was low, as shown by the number of EdU^+ acinar cells after the 2-hour chase being similar to that after 7 days (Fig. 1D and fig. S1E). In contrast, we found extensive acinar cell proliferation at 7 days post-IR (day 7 + 2 hours), with a fourfold increase ($P < 0.001$) in the number of EdU^+ cells at this time point compared to non-IR controls (Fig. 1E and fig. S1F). Moreover, these cells underwent substantial turnover, as demonstrated by the significant reduction in EdU^+ acinar cells after the 7-day chase (>2-fold decrease; $P < 0.0001$; Fig. 1E and fig. S1F). In comparison, active acinar cell turnover at 14 days post-IR was greatly diminished. Although the 2-hour chase suggested that the 14-day post-IR glands had similar levels of cell division to that of homeostatic non-IR glands (Fig. 1F and fig. S1G), we found an 84% increase ($P < 0.001$) in EdU^+ acinar cells after the 7-day chase, suggesting that originally EdU-incorporated acinar cells had undergone a round of cell replication but did not undergo further cell division (Fig. 1F and fig. S1G). Thus, these results are consistent with both our $pHH3^+$ quantification and transcriptomic analysis and confirm that salivary glands undergo an early phase of active acinar cell proliferation and replacement in response to IR that is lost by 14 days.

Given the known role of parasympathetic nerves in salivary gland secretory function and acinar cell replacement (*10*, *32*), we next asked whether the functional nerve supply to acini was altered at 7 or 14 days post-IR compared to non-IR controls. Bulk RNA sequencing (RNA-seq) analysis identified a significant up-regulation of genes involved in neuronal patterning, nerve migration, and neurogenesis (*Nrg1*, *Nedd4*, *Nrp1*, *Nrp2*, *Robo1*, and *Cyfip1*) (*33*, *34*), synapse assembly/activity (*Stmn1*) (*35*), and nerve function (*Vip*) (*10*) at 7 days post-IR, suggesting that radiation exposure activates neuronal programs at the same time as acinar cell replacement (Fig. 1, A and B). We also found the muscarinic receptor 1 (*Chrm1*), which upon activation promotes proliferative signaling in acinar progenitors and a subset of transit-amplifying cells (*36*), to be up-regulated (Fig. 1A), an outcome suggestive of an increase in nerve–acinar cell communication at 7 days post-IR. However, by 14 days post-IR, neuronal genes were reduced, with levels returning to those of non-IR controls, indicating a return to homeostatic innervation.

Next, we analyzed changes in nerve–acinar cell function by measuring physiological saliva output at 7 and 14 days post-IR through the induction of the gustatory-salivatory reflex (*37*). The gustatory-salivatory reflex involves afferent input from the tongue to the dorsal medulla that synapse with parasympathetic neurons innervating the salivary gland, with stimulation of these nerves driving saliva secretion (*38*, *39*). Gustatory nerves were stimulated through the local application of citric acid to the tongue, and saliva was collected over 20 min, as performed previously (*39*). Saliva output from mice at both 7 and 14 days post-IR was similar to that from non-IR controls (Fig. 1G), suggesting that radiation does not damage parasympathetic nerve–acinar cell interactions or nerve function at these time points. This was further confirmed by immunofluorescent analysis, followed by surface rendering using Imaris image analysis software, revealing similar levels of $GFRa2^+$ parasympathetic nerves in close proximity to acini at 14 days post-IR and in non-IR controls (Fig. 1, H and I). However, similar to previous findings (*40*), direct stimulation of saliva secretion from acinar cells through systemic injection of the synthetic global muscarinic agonist (can activate *Chrm1* to *Chrm5*) pilocarpine revealed a 20% reduction in maximal saliva output (totaling all three major salivary glands) at 14 days, but not at 7 days, post-IR ($P < 0.01$; fig. S1H), confirming previously described, specific pilocarpine-stimulated secretory dysfunction by 2 weeks post-IR as a result from damage to muscarinic receptor–coupled signal transduction in parotid acinar cells (*41*).

Acinar cells remain receptive to muscarinic-induced proliferation 14 days post-IR, with local delivery of a CV ALG extending the time period of cell division

Using an ex vivo salivary gland (sublingual) organoid model, we previously showed that muscarinic receptor activation within the first 48 hours following IR exposure results in the repopulation of acini by $SOX2^+$ progenitor cells (Fig. 2A) (*10*). However, whether irradiated acinar cells remain receptive to muscarinic receptor–induced proliferation weeks after IR exposure is unknown. To test the regenerative potential of acinar cells, we subcutaneously administered the muscarinic agonist CV locally to the neck region overlying both the submandibular and sublingual glands (Fig. 2, B and C) at 14 days post-IR. The 14-day post-IR time point was chosen on the basis of the reductions seen in acinar cell turnover and pilocarpine-induced maximal saliva output, as compared to that at 7 days post-IR (Fig. 1, F and G, and fig. S1E). In addition, this delay allows for defining the response of salivary tissues to the muscarinic agonist weeks after radiation treatment. Given that the identity of acinar progenitors is known in the sublingual but not the submandibular gland, we first quantified the number in $pHH3^+SOX2^+$ acinar progenitor cells and their progeny, the $pHH3^+SOX2^-$ transit-amplifying cells, in response to CV at 18 hours, 3 days, and 7 days after administration (Fig. 2D). As shown in Fig. 2E, local delivery of free CV significantly induced acinar cell proliferation 18 hours after administration, with a 1.8-fold increase in $pHH3^+SOX2^+$ progenitors (white arrows; cell number shown as a percentage of the total number of acinar nuclei) and a 4.5-fold increase in $pHH3^+$-$SOX2^-$ transit-amplifying acinar cells (white arrowheads) compared to saline-treated controls (Fig. 2E and fig. S2A). However, cell proliferation returned to baseline (saline) levels by 3 days after CV administration (Fig. 2E, CV), thereby demonstrating that acinar cells are still receptive to muscarinic-driven proliferation but that a single injection of free CV–mediated cell cycle entry is highly transitory.

Given this result, we next asked whether sustained release of CV via incorporation into an ALG could promote a longer period of mitotic activity compared to free CV. Alginate is a biocompatible, naturally occurring polymer that is considered safe for drug delivery (*42*) and has been used in various drug release settings (*43*–*45*). Biodegradability of the alginate was achieved by oxidizing the alginate as previously described (*46*). Similar to pilocarpine (*45*), CV forms

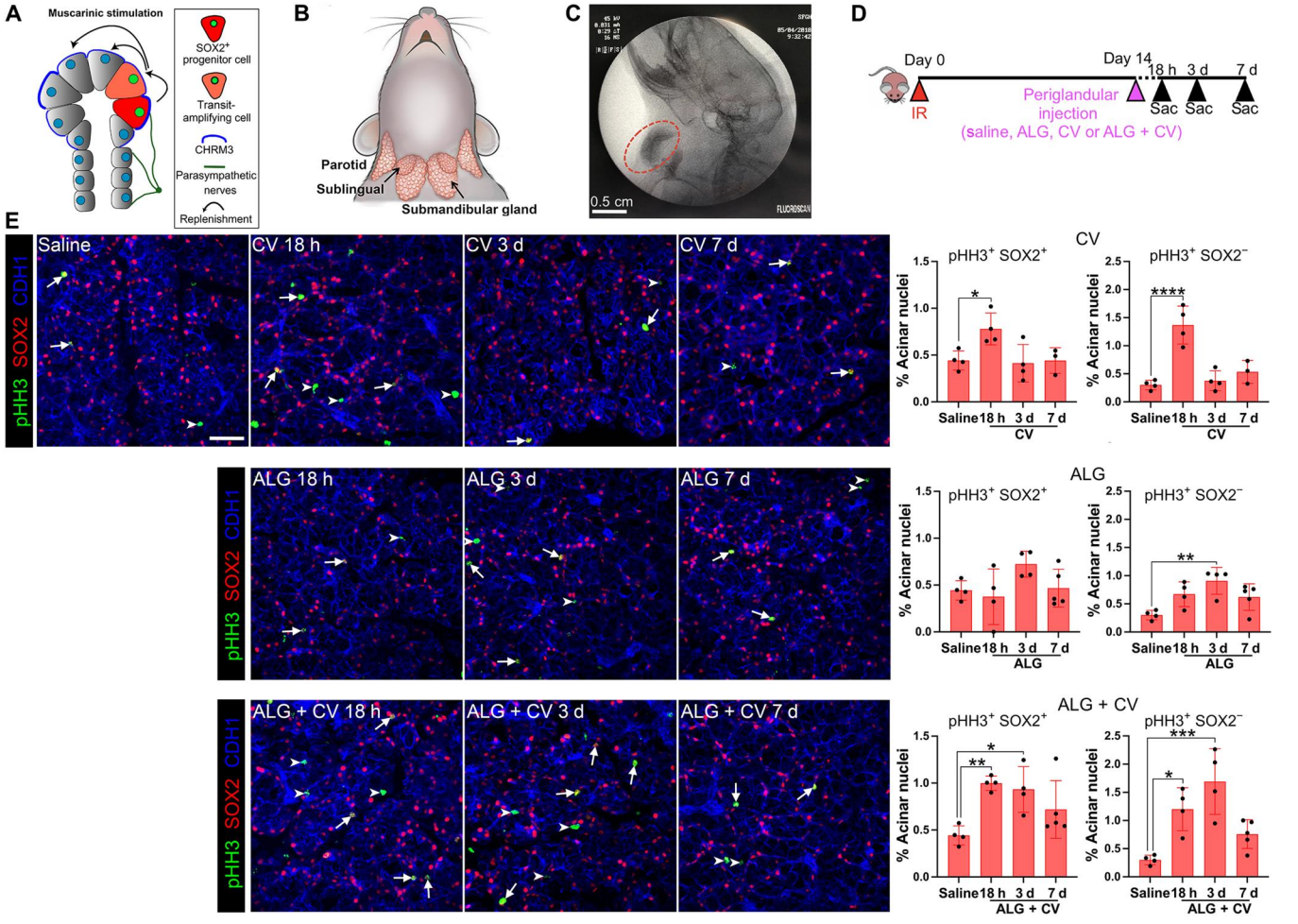

Fig. 2. CV, free or incorporated into an ALG, stimulates acinar cell replenishment 2 weeks after radiation. (**A**) Schematic showing that salivary acinar replacement in healthy tissue is regulated by parasympathetic innervation. Upon muscarinic stimulation, SOX2$^+$ progenitor cells divide and produce daughter acinar cells. (**B**) Location of the major murine salivary glands: parotid, submandibular, and sublingual. (**C**) ALG was delivered via injection into the area immediately adjacent to the salivary glands and imaged via x-ray (Fluoroscan). ALG is marked by a red circle. (**D**) Radiation and treatment regimen. Salivary glands were collected and analyzed 18 hours, 3 days, and 7 days after treatments with saline, CV, or CV + ALG. (**E**) Immunofluorescent analysis of SOX2$^+$ acinar progenitors and SOX2$^-$ transit-amplifying acinar cells from different treatment conditions [shown in (D)] using antibodies to the mitotic marker, phospho-histone H3 (pHH3, green), SOX2 (red), and the epithelial marker, E-cadherin (CDH1, blue). Arrows point to pHH3$^+$ SOX2$^+$ cells, and arrowheads point to pHH3$^+$ SOX2$^-$ cells. Scale bar, 40 μm. Dots in the bar graphs represent biological replicates. Data are expressed as means ± SD. *P < 0.05; **P < 0.01; ***P < 0.001; ****P < 0.0001; a one-way ANOVA with Dunnett's multiple comparison test was applied.

noncovalent interactions with oxidized alginate through charge interactions between the tertiary amine (positive charge) and carboxylate (negative charge) and may form H bonds with the aldehyde group (fig. S2B) to delay diffusion from the hydrogel. In vitro release of the CV from the ALG hydrogels was maintained for at least 2 days (fig. S2C).

To test the functional benefit of the hydrogel for delivery in vivo, ALG or ALG + CV was injected subcutaneously and periglandularly (sublingual and submandibular) at 14 days post-IR (Fig. 2C). While the envisioned delivery would be intraglandular, the small size of the rodent glands required periglandular delivery to evaluate in vivo function. Upon delivery, cell proliferation was measured 18 hours, 3 days, and 7 days later. As shown in Fig. 2E (bottom), a single dose of ALG + CV significantly increased both SOX2$^+$ progenitor and SOX2$^-$ transit-amplifying cell proliferation at both 18 hours (2- and 4-fold, respectively) and 3 days (~2- and ~5-fold, respectively) compared to saline-treated controls, with increased cell proliferation remaining at 7 days, albeit not significantly (Fig. 2E, ALG + CV). Notably, ALG by itself was also able to promote cell proliferation (Fig. 2E, ALG), although this was only significantly increased in SOX2$^-$ transit-amplifying cells at 3 days after injection (threefold; P < 0.01; Fig. 2E, ALG graph). To ensure that muscarinic agonist–induced acinar cell proliferation was not restricted to the sublingual gland, we also quantified pHH3$^+$MUC10$^+$ serous acinar cells in the submandibular gland (fig. S2, D and E) and found a significant increase in cell division at 18 hours and 3 days after injection of ALG + CV [2.4-fold (P < 0.01) and 2.3-fold (P < 0.05) increase, respectively], with the values returning to baseline by 7 days (fig. S2E). Together, these data demonstrate that sublingual and submandibular acinar cells can still be induced to divide in vivo at 2 weeks post-IR through stimulation of muscarinic receptors and that the effect of this

mitotic agent can be extended up to at least three to seven subsequent days through the incorporation of CV into an ALG.

A single dose of ALG + CV transiently rescues saliva secretion and reduces glandular degeneration after radiation

Given the proliferative response of irradiated acinar cells to CV, we next asked whether a single dose of CV or ALG + CV at 14 days post-IR could maintain saliva secretion and salivary gland architecture over a 10-week time period. This 10-week time frame was chosen on the basis of rodent models showing extensive salivary gland degeneration 8 to 12 weeks after radiation exposure (*14*). Mice were irradiated at day 0 and treated with ALG + CV, free CV, ALG only, or saline (control) 14 days later, and levels of citrate-driven (nerve-mediated) saliva output were measured each week through gustatory stimulation (Fig. 3A). A maximal (pilocarpine-driven) saliva secretion assay was also performed at 68 days, and tissue was then extracted for immunofluorescent analysis at 70 days (10 weeks; Fig. 3A).

As shown in Fig. 3B, saline-treated IR (control) mice maintained physiological saliva secretion at non-IR levels until 41 days post-IR (6 weeks), when a significant decrease was measured (30%, $P < 0.05$), an outcome sustained over the following weeks. In contrast, IR mice treated with free CV or ALG + CV were able to maintain secretory output at similar levels to the non-IR controls beyond 41 days post-IR (Fig. 3B). At 49 days post-IR, both CV- and ALG + CV–treated mice showed significantly increased saliva secretion compared to saline-treated IR mice (87% and 78% increase, respectively; $P < 0.05$). However, only ALG + CV treatment was able to significantly maintain saliva output at non-IR levels by day 56 (68% increase compared to saline IR controls, $P < 0.05$) (Fig. 3B), suggesting that local, sustained release of CV from the hydrogel promotes extended functional recovery. By day 63, however, saliva secretion from ALG + CV–treated mice was similar to that from saline IR mice, indicating that physiological function was no longer preserved (Fig. 3B). Similarly, maximal saliva secretion from all irradiated mice (saline control or treated) was reduced below non-IR controls at day 68 (Fig. 3C). Notably, maximal saliva levels in irradiated mice at day 68 were not significantly different from those at 14 days post-IR, suggesting that the level of tissue damage at this later time point did not further reduce muscarinic receptor–mediated saliva output. Thus, while a single dose of ALG + CV and CV treatment maintains physiological saliva output up to 8 weeks post-IR, it is not capable of preserving saliva secretion in the long term.

We next proceeded to analyze salivary glands for alterations in tissue structure and function by measuring changes in secretory cell number and secreted protein synthesis. Given that the submandibular gland is responsible for at least 60% of saliva secretion in rodents (*47*) and its serous acini are severely damaged by IR (*14*), we first focused on acinar cell architecture and protein biosynthesis within this gland type by immunostaining for the water channel aquaporin 5 (AQP5) and the secreted protein mucin 10 (MUC10). Consistent with the known degeneration of irradiated submandibular glands 8 to 12 weeks after IR exposure (*14*), saline- and ALG-treated tissue showed extensive destruction of functional acini at 70 days (10 weeks) post-IR (fig. S3A), with a 50% decrease in both the number of $AQP5^+$ ($P < 0.0001$; Fig. 3, D and E) and $MUC10^+$ acinar cells ($P < 0.0001$; Fig. 3, F and G). In comparison to non-IR glands, CV-treated glands showed only a 37% reduction in $AQP5^+$ acinar cells ($P < 0.001$; Fig. 3, D and E) and a 33% decrease in $MUC10^+$ acinar cells ($P < 0.001$; Fig. 3, F and G), suggesting that the short (18-hour) induction of cell proliferation with CV alone at 14 days post-IR (fig. S2D) already positively affected acinar cell number. However, preservation of secretory acini was even more pronounced in ALG + CV–treated glands, with only a 20% reduction ($P < 0.01$) in the number of $AQP5^+$ and $MUC10^+$ acinar cells compared to non-IR glands (Fig. 3, D to G), suggesting that the longer-term induction of cell proliferation after delivery of ALG + CV at 14 days post-IR (fig. S2D) significantly maintains acinar cells beyond the IR-induced degeneration phase (>8 weeks).

Given these outcomes, we next determined whether acinar progenitors remained in a regenerative state at 70 days post-IR. Although mucous acini are less susceptible to IR-induced destruction compared to serous cells (*12*, *48*), due to the known identity of acinar progenitor cells in the sublingual gland but not in the submandibular gland, we focused on the former gland type. Notably, IR glands treated with ALG + CV, but not ALG or CV, showed a significant increase in dividing acinar cells, with a 5-fold increase in $pHH3^+SOX2^+$ progenitors ($P < 0.01$) and a 10-fold increase in $pHH3^+SOX2^-$ transit-amplifying ($P < 0.01$) cells compared to saline-treated IR controls (Fig. 3, H to J). However, despite ALG + CV promoting progenitor cell proliferation, the overall number of $SOX2^+$ progenitors was unchanged compared to non-IR controls (Fig. 3K), suggesting that $SOX2^+$ cells are likely activated to undergo asymmetric division. Thus, these data indicate that despite the reduction in salivary gland secretory function by 10 weeks, acinar cells continue to proliferate in irradiated glands in response to ALG + CV, resulting in improved acinar cell number and glandular integrity.

Given that parasympathetic nerves regulate physiological saliva secretion and acinar cell replacement (*10*, *49*), we next determined whether CV treatment preserved parasympathetic innervation of the acini. In the salivary glands, thick nerve bundles travel alongside ducts, and axons begin to separate (i.e., defasciculate) as they innervate individual acini. However, during injury, axons degenerate or retract (*50*), resulting in the appearance of thicker nerve bundles and reduced innervation of secretory cells. Therefore, to detect changes in neuronal presence, we quantified the number of thin (<1.5 μm in diameter) $GFRa2^+$ nerve filaments within the acinar compartment using Imaris surface rendering and filament tracing tools (fig. S3B). Consistent with tissue injury, we measured a significant reduction in the number of thin $GFRa2^+$ filaments innervating the acini of saline-treated (70% decrease; $P < 0.05$) and ALG-treated mice (78% decrease; $P < 0.01$) compared to non-IR controls (Fig. 3, L and M, and fig. S3B), indicating that IR results in acinar cell denervation by this time point. Innervation of acini was also substantially reduced in CV-treated mice ($P < 0.05$), with a 60% decrease in $GFRa2^+$ axon filaments compared to non-IR tissue (Fig. 3, L and M, and fig. S3B). Notably, however, innervation of ALG + CV acini was similar to that of the non-IR controls (Fig. 3, L and M, and fig. S3B), suggesting that, despite the loss in physiological saliva secretion, nerve-acinar interactions remained intact. To ensure that acinar cells within ALG + CV–treated glands remained capable of receiving signals through the muscarinic pathway, tissue was immunostained at 70 days post-IR for the muscarinic receptor CHRM3 (*51*), the key driver of acinar cell secretion. We found CHRM3 levels in the acinar cells of ALG + CV–treated glands to be similar to those in

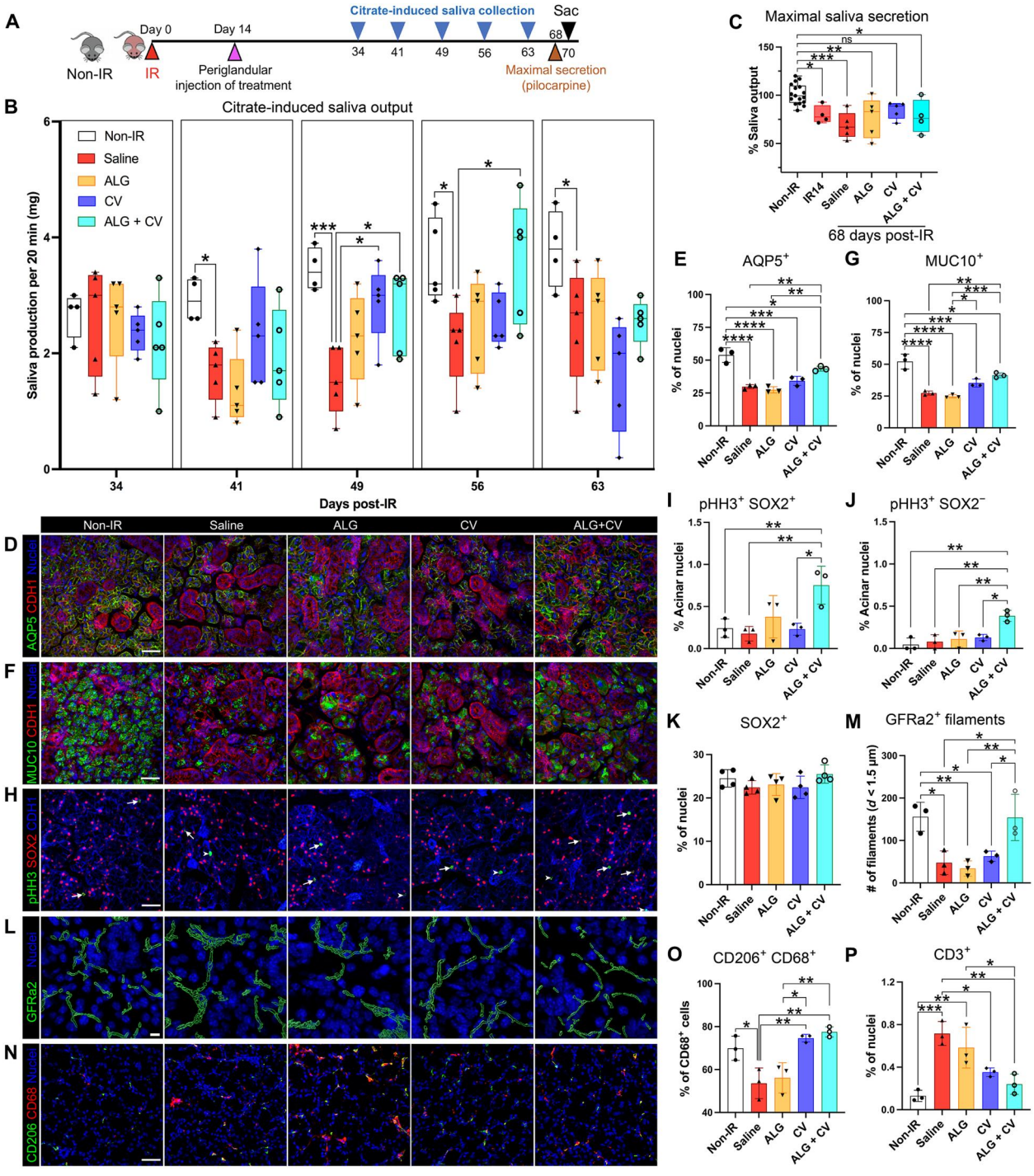

Fig. 3. A single dose of ALG + CV transiently rescues saliva secretion and reduces glandular degeneration after radiation. (**A**) Regimen for radiation, treatment, and saliva collections. (**B**) Physiological saliva output levels were measured weekly from 34 to 63 days post-IR using gustatory stimulation (citric acid applied to tongue). (**C**) Maximal saliva secretion in response to systemic pilocarpine administration at 68 days. Data were normalized to non-IR controls. ns, not significant. (**D** to **G**) Representative images and quantification of acinar cells expressing AQP5 (D and E) or the secreted protein MUC10 (F and G). E-cadherin (CDH1, red) marks all epithelial cells. Nuclei are stained with Hoechst 33342 (blue). (**H** to **K**) Representative images (H) and quantification of mitotic (pHH3$^+$, green) acinar progenitor cells (I) (SOX2$^+$, red) and transit-amplifying cells (J) (SOX2$^-$) and the total number of SOX2$^+$ cells (K). (**L** and **M**) Representative images (L) and quantification (M) of GFRa2$^+$ parasympathetic nerve filaments (green). GFRa2$^+$ filaments with diameters of less than 1.5 μm (innervating the acini) were quantified. (**N** to **P**) Representative images of macrophages (M) and quantification of M2-polarized CD68$^+$CD206$^+$ macrophages (O) and CD3$^+$ T cells (P). Scale bars, 40 μm (D, F, H, and N) and 10 μm (L). Dots in the graphs represent biological replicates. Data are expressed as means ± SD. *P < 0.05; **P < 0.01; ***P < 0.001; ****P < 0.0001; a one-way ANOVA with Dunnett's multiple comparison test was applied for all graphs except in (B); a two-way ANOVA with Dunnett's multiple comparison test was applied to (B).

non-IR cells (fig. S3C), indicating that muscarinic receptor expression was maintained but that acinar cells had reduced secretory function in response to cholinergic signals.

On the basis of the fact that parasympathetic nerves can promote an anti-inflammatory environment (*52*), we next questioned whether CV also affected immune cell infiltration at 70 days. We found a marked change in inflammatory cells in irradiated tissue treated with saline or ALG compared to non-IR controls (Fig. 3, N to P, and fig. S3, D to F). With respect to the innate immune response, all irradiated tissues, regardless of treatment, demonstrated a significant increase in the total number of $CD68^+$ macrophages ($P < 0.01$, pan-macrophage marker; fig. S3, E and F). However, the ratio of pro-reparatory M2 ($CD68^+$ $CD206^+$) to proinflammatory M1 ($CD68^+$ $CD206^-$) macrophages (*53*) was significantly elevated in ALG + CV− and CV-treated tissues compared to saline-treated IR salivary glands (Fig. 3O). As expected from previous studies (*54*), we found a fivefold increase in the number of $CD3^+$ T cells in saline- and ALG-treated mice, suggestive of activation of degenerative processes ($P < 0.001$ for saline and $P < 0.01$ for ALG; Fig. 3P and fig. S3C). However, mice treated with either ALG + CV or CV showed significantly fewer $CD3^+$ T cells compared to saline IR controls (threefold decrease, $P < 0.05$ and twofold decrease, $P < 0.01$, respectively) and were not significantly different from non-IR glands (Fig. 3P). Together, these outcomes suggest that CV promotes an anti-inflammatory/pro-reparatory environment.

In summary, despite saliva secretion not being fully restored, these data indicate that slow release of ALG + CV preserves the acinar compartment by promoting proliferation and maintaining the surrounding nerve supply while activating pro-repair immune responses.

Multiple doses of CV maintain physiological saliva secretion, acinar cell architecture, and functional innervation in the long term

Given that a single dose of ALG + CV at 14 days post-IR was able to improve secretory function, albeit transiently, and reduce the loss of acini and their cholinergic nerve supply, we next asked whether multiple doses could lead to a sustained improvement in glandular function and structure. Because of the subcutaneous alginate minimally degrading over time, with the biogel remaining present at 70 days post-IR, we proceeded to administer the initial treatment of ALG + CV, ALG, or saline at 14 days post-IR and follow this with weekly local injections of CV into the ALG + CV mice (ALG + multiCV) and saline into the saline- or ALG-treated mice, starting at 38 days post-IR (i.e., 3 weeks after the initial saline, ALG, and ALG + CV at 14 days). This time point was chosen on the basis of the saline-treated mice showing a significant reduction in physiological saliva secretion at 41 days post-IR (Fig. 3B). Physiological salivary function was then measured every 2 weeks from days 35 to 91 post-IR via gustatory stimulation (Fig. 4A). As for the mice receiving a single dose, both saline- and ALG-treated mice undergoing multiple dosing showed reduced physiological saliva secretion, with a reduction of 62% ($P < 0.001$) and 34% ($P < 0.08$), respectively, by 49 days post-IR (Fig. 4B). In contrast, our multidose regimen resulted in ALG + multiCV–treated mice having saliva secretion levels that mimicked those of non-IR mice, and were significantly above those of IR mice, for the entire 3 months (91 days) measured (Fig. 4B), indicating that ALG + multiCV was sufficient to restore physiological saliva secretion in the long term.

We next determined the extent to which the acinar compartment was damaged in the different treatment groups by performing a maximal saliva secretion assay through systemic injection of pilocarpine. Both saline- and ALG-treated mice exhibited a significant reduction in maximal saliva production upon stimulation at 92 days compared to non-IR mice (50%, $P < 0.0001$ and 43%, $P < 0.0001$ of non-IR levels, respectively) as well as compared to 14-day post-IR mice [40% reduction ($P < 0.01$) for saline and 29% ($P < 0.05$) for ALG; Fig. 4C]. Although saliva secretion for ALG + multiCV–treated mice did not completely mimic those of non-IR controls (30% decrease; $P < 0.0001$), maximal secretory function had a significant 36% increase compared to that for saline-treated IR mice ($P < 0.05$; Fig. 4C). Furthermore, the maximal secretion level was not significantly different from that of mice at 14 days post-IR (Fig. 4C), suggesting that ALG + multiCV treatment halts additional gland injury after this time point. Thus, ALG + multiCV substantially aids in the retention of physiological cell function and is able to maintain maximal secretion from radiation-injured tissue from the time of treatment.

On the basis of the preservation of saliva output with ALG + multiCV treatment, we next determined whether acinar cell architecture was also positively affected through immunofluorescent analysis (fig. S4A). As with the 70-day post-IR submandibular gland, we found the acinar cell compartment to be significantly preserved by ALG + multiCV treatment, with only a 20% reduction in the $AQP5^+$ acinar cells compared to non-IR controls ($P < 0.0001$), whereas saline- and ALG-treated tissue showed a 46% and 54% decrease ($P < 0.0001$) in acinar cell number, respectively (Fig. 4, D and E). Furthermore, in contrast to the large reduction (>40% decrease) in MUC10-synthesizing acinar cells in saline-treated ($P < 0.01$) and ALG-treated ($P < 0.001$) glands, the number of $MUC10^+$ cells in ALG + multiCV–treated tissue was significantly increased compared to that of saline-treated IR mice and mirrored that of the non-IR controls (71%; $P < 0.01$; Fig. 4, F and G), suggesting that ALG + multiCV serves to maintain secretory protein–secreting acinar cells.

Given the extensive preservation of acinar cells with ALG + multiCV treatment (Fig. 4, D to G), we next questioned the impact of the various treatments on the expansion of the global acinar cell pool and the proliferation status of its progenitors at the 93-day post-IR time point. We found that the total number of $SOX2^+$ acinar progenitors in saline-treated ($P < 0.01$) and ALG-treated ($P < 0.001$) IR tissue was significantly lower than in non-IR control glands (Fig. 4K), confirming that acinar progenitors are not maintained post-IR. Unexpectedly, we measured a significant increase in proliferating $pHH3^+SOX2^+$ cells in saline-treated IR glands as compared to non-IR tissue (10-fold, $P < 0.001$; Fig. 4, H and I). However, the number of $pHH3^+SOX2^-$ transit-amplifying cells was reduced (Fig. 4J), suggesting that $SOX2^+$ progenitors do not undergo active cell division to produce differentiated daughter cells. In contrast to saline or ALG treatment, ALG + multiCV treatment not only significantly increased the number of $pHH3^+SOX2^+$ progenitors (12-fold compared to non-IR glands; $P < 0.0001$; Fig. 4, H and I) but also expanded the number of $pHH3^+SOX2^-$ transit-amplifying cells (2-fold increase over saline-treated IR glands, $P < 0.05$; Fig. 4J) while maintaining the $SOX2^+$ progenitor population equal to that in non-IR glands. Thus, these data indicate that

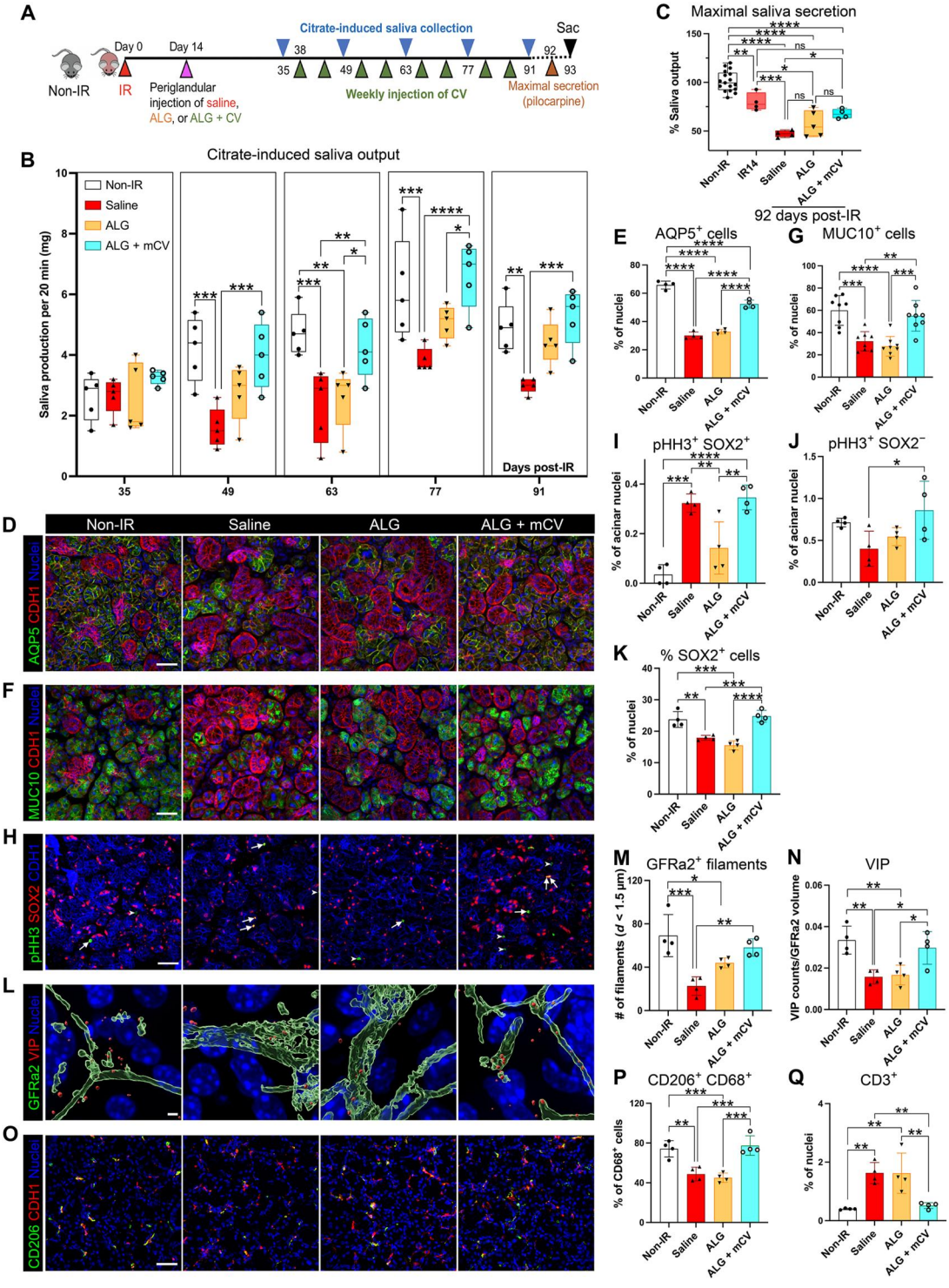

Fig. 4. Multiple doses of CV maintains physiological saliva secretion, acinar cell architecture, and functional innervation in the long term. (**A**) Timeline for radiation, treatments, and saliva collections. (**B**) Citrate-induced saliva output was measured once every 2 weeks from 35 to 91 days after radiation. (**C**) Maximal saliva secretion in response to systemic pilocarpine administration at 92 days. Data were normalized to non-IR controls. (**D** to **G**) Representative images and quantification of AQP5$^+$ (D and E) and MUC10$^+$ (F and G) acinar cells. Epithelial cells and nuclei were stained for E-cadherin (CDH1, red) and nuclei (Hoechst 33342, blue). (**H** to **K**) Representative images (H) and quantification of mitotic (pHH3$^+$) acinar progenitor cells (I) (SOX2$^+$) and transit-amplifying cells (J) (SOX2$^-$). Quantification of SOX2$^+$ acinar cells is shown in (K). (**L** to **N**) Representative images (L) and quantification of parasympathetic nerves marked by GFRa2 (M) [green, three-dimensional (3D) surface reconstructed with Imaris] and the neuropeptide VIP (N) (red, 3D surface reconstructed using Imaris). Hoechst 33342, nuclei (blue). GFRa2$^+$ filaments with diameters of less than 1.5 μm (innervating the acini) were quantified. VIP was normalized to GFRa2$^+$ filament volumes. (**O** to **Q**) Representative images (O) and quantification of pro-reparative (CD68$^+$CD206$^+$) M2-polarizing macrophages (P) and CD3$^+$ T cells (Q). Scale bars, 40 μm (D, F, H, and O) and 10 μm (L). Dots in the bar graphs represent biological replicates. Data are expressed as means ± SD. *P < 0.05; **P < 0.01; ***P < 0.001; a one-way ANOVA with Dunnett's multiple comparison test for all graphs except in (B); a two-way ANOVA with Dunnett's multiple comparison test was applied to (B).

ALG + multiCV not only is able to increase the pool of actively dividing SOX2$^+$ progenitors for the repopulation of the progenitor cell pool but also ensures a large population of proliferating transit-amplifying cells that ultimately replenishes the acinar cell compartment.

Similar to our analysis at 70 days post-IR, we found ALG + multiCV treatment to substantially rescue functional parasympathetic innervation of secretory acini. Innervation of acinar cells by thin GFRa2$^+$ filaments (diameter, <1.5 μm) closely resembled that of non-IR glands (Fig. 4L and fig. S4C), whereas GFRa2$^+$ filaments in saline-treated tissue only reached 40% of non-IR levels (P < 0.001; Fig. 4M). Furthermore, consistent with the gustatory-stimulated saliva secretion outcomes (Fig. 4B), parasympathetic nerve function was also maintained, as shown by the levels of

vasoactive intestinal peptide (VIP), a key prosecretory neuropeptide (*55*), being similar in both ALG + multiCV–treated and non-IR salivary glands, and significantly greater than in the saline IR controls (twofold; $P < 0.01$; Fig. 4, L and N, and fig. S4D). Although ALG treatment also showed some increase in innervation of acini (Fig. 4, L and M, and fig. S4D), the levels of VIP resembled that of saline controls (Fig. 4N and fig. S4D), indicating that ALG alone does not rescue nerve function.

Last, we questioned immune cell infiltration in response to the different treatments at 93 days post-IR. Similar to the 70-day post-IR tissue, IR significantly increased the total $CD68^+$ pan-macrophage population within the glands under all treatment conditions ($P < 0.001$ for saline and ALG + multiCV; $P < 0.0001$ for ALG; fig. S4B). However, only ALG + multiCV–treated salivary glands contained significantly higher numbers of pro-reparatory $CD206^+$ M2 macrophages (fig. S4B), with the percentage of $CD206^+CD68^+$ macrophages (of the total $CD68^+$ cells) being significantly increased compared to saline-IR salivary glands (60% increase; $P < 0.001$) and similar to non-IR controls (Fig. 4, O and P). We also found the number of $CD3^+$ T cells in ALG + multiCV–treated tissue to resemble that of non-IR controls, contrasting greatly with the substantial infiltration of $CD3^+$ T cells (threefold increase; $P < 0.01$) into saline- and ALG-treated glands (Fig. 4Q and fig. S4E). Together, these studies indicate that extending the delivery time of CV is sufficient to maintain long-term physiological saliva output, improve tissue architecture, and promote a pro-repair environment in response to radiation damage (Fig. 5).

DISCUSSION

Despite the vast array of tissues inadvertently damaged by radiation treatment for cancers, with salivary glands being one of the most frequently injured tissues (*56*), regenerative therapies capable of restoring organ architecture and physiological function have remained elusive. We and others have demonstrated that nerves are critical regulators of somatic stem cell behavior (*10*, *57*, *58*), but to date, it was unknown whether they also mediate regenerative responses after radiation-induced damage and, if so, by what mechanism(s). Here, we show that local administration of a muscarinic receptor agonist to irradiated salivary glands promotes acinar cell replacement, maintains tissue architecture and parasympathetic innervation, and restores secretory function over an extensive time course, thereby preserving physiological levels of saliva necessary for oral and systemic well-being (see Fig. 5). Together, our data indicate that irradiated epithelial tissues have the capacity to respond to pro-regenerative treatments, potentially months after radiation treatment in humans, and support the application of this injectable hydrogel therapy for reversing salivary gland dysfunction after radiation-induced damage.

Acinar cell degeneration is the most prominent outcome of radiation-induced damage to salivary glands (*13*, *48*), resulting in the loss of saliva protein synthesis and fluid secretion. Unexpectedly, however, very few studies to date have been actively engaged in directly promoting acinar cell replacement after radiation damage. Rather, strategies have been based on preserving acinar cells through inhibition of apoptosis (*59*) and senescence (*60*), restoring healthy tissue through the application of stem cell–derived organoids that contain acinar cells (*61*, *62*), and the deletion of damaged cells (*63*). Here, we demonstrate that the acinar cell pool can be directly regenerated through activation of muscarinic receptors enriched on the acinar progenitors, thus repopulating the glands with functional secretory acini. Muscarinic receptor signaling has previously been shown to promote stem cell expansion (*10*, *64*) and epithelial cell division (*64*, *65*) in other organ systems. Specifically, in the salivary gland, it induces extensive acinar cell proliferation in uninjured conditions in vivo (*10*), as well as in ex vivo explants immediately after radiation (*10*). However, this is the first in vivo study to reveal that acinar cell replacement can be activated weeks to months after radiation damage, preventing further degeneration of the acinar cell compartment and preserving physiological saliva secretion. Given that a single dose and fractionated doses of radiation result in acinar cell degeneration at the later

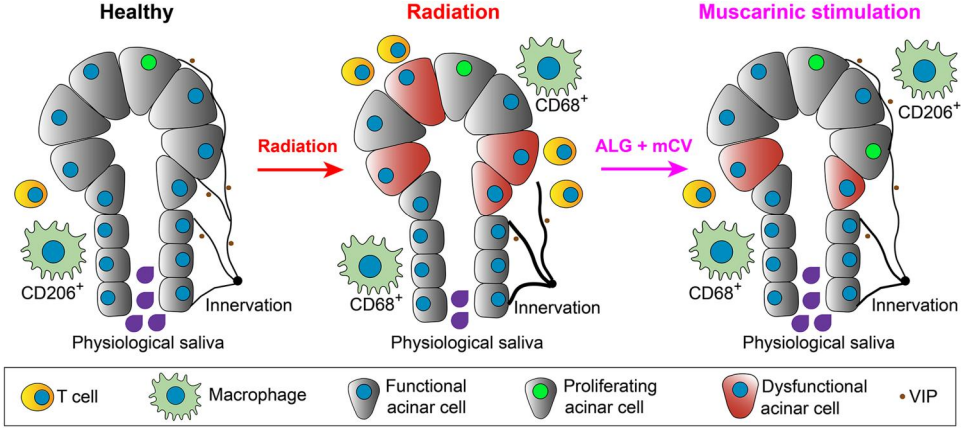

Fig. 5. Model of muscarinic-induced acinar cell regeneration. Under healthy conditions, salivary acinar cells (green) are highly secretory and extensively innervated by parasympathetic axons (black) that regulate both cellular function and tissue homeostasis through the production of neurotransmitters, e.g., VIP, black dots. Upon radiation damage, salivary gland acinar cells undergo degeneration, acinar progenitor cells are reduced in number, functional parasympathetic innervation of acini is lost, and the tissue is infiltrated by T cells and macrophages that are polarized toward proinflammatory phenotypes (e.g., $CD68^+CD206^-$). However, treatment of irradiated glands with the muscarinic agonist CV, encapsulated in an ALG, reverses these outcomes, resulting in acinar cell regeneration, the maintenance of acinar progenitor cells, a pro-repair immune response, and the restoration of innervation and glandular function.

stages, we predict that glandular regeneration in response to muscarinic agonism will be similar for both dosing strategies. However, further studies are needed to determine whether this is the case.

Little is known about the ability of acinar cells to renew after radiation, other than their capacity to undergo increased cycling up to 20 days post-IR (*66*). This cellular response has been confirmed by genetic lineage tracing studies in mice where recombination is activated in acinar cells before IR, with glands showing active replenishment of acinar cells within 14 days [marked by *Sox2* (*10*)] or up to 90 days [marked by *Mist1* (*67*)] post-IR. Human salivary gland acinar cells may also have regenerative potential, as, despite the severe loss in acini at 2.4 months post-IR, small clusters of acinar cells still express proliferative and functional markers after >10 years of post-radiotherapy treatment (*15*). However, in all cases, endogenous replenishment is not sufficient to maintain organ structure and function post-IR, with all rodents and human patients ultimately showing loss of saliva output. Our findings confirm that such spontaneous proliferation in $SOX2^+$ acinar cells can occur up to 70 to 90 days post-IR but is unable to maintain the overall $SOX2^+$ acinar progenitor cell pool necessary to repopulate the injured gland. To date, it remains unclear what signal(s) induces the initial cycling of acinar progenitors after radiation and why this is lost over time. Our data demonstrating that the maintenance of muscarinic receptor activation in irradiated glands is sufficient to sustain acinar cell proliferation and the overall acinar cell pool over the long term, and the known pro-proliferative role of muscarinic agonism, suggest that this pathway is a key regulator of cell regeneration. The downstream pathways that muscarinic receptors activate to promote acinar cell proliferation in the glands remain unclear. CHRM1 and CHRM3 have been shown to activate multiple signaling pathways, including epidermal growth factor receptor (EGFR)/extracellular signal–regulated kinase (ERK) (*68*), protein kinase C (PKC)/Ca^{2+} (*69*), and phosphatidylinositol 3-kinase (PI3K)–AKT–mTOR (*70*), to drive a diverse array of cellular functions including cell division and differentiation. However, further studies are needed to determine why endogenous muscarinic agonism fails over time and whether other signaling systems, in addition to muscarinic receptors, are involved. Furthermore, whether removal of CV after 3 months of treatment returns the gland to a self-sustaining state requires further investigation.

Replenishment of the acinar cell pool not only is essential for tissue repair but also requires maintenance of the surrounding nerve-enriched niche that influences secretion and organ homeostasis (*49*). With the ablation of parasympathetic nerve function resulting in acinar cell atrophy and the absence of saliva (*10*, *71*, *72*), the severe reduction in parasympathetic innervation of human salivary glands 2 years after radiation therapy (*11*), and the reduction in acinar cell innervation 2 to 3 months after radiation, as revealed in this study, is likely a significant mediator of irreversible degeneration. The ability of CV, when administered weekly, to preserve this essential, functional interaction allows for the acquisition of a near-homeostatic state. How CV acts to sustain this positive feedback loop between nerves and acini remains unclear. It is well known that nerve–target cell interactions are initiated and maintained by neurotrophic factors produced by the target cells (*73*), including acinar cells. The neurotrophic factor neurturin (NRTN), a key regulator of acinar cell innervation by parasympathetic nerves during salivary gland development (*11*), increases innervation when overexpressed in irradiated adult tissue (*74*) and is significantly reduced in irradiated adult human acinar cells (along with the nerves) (*11*). Although it is not known whether muscarinic receptors specifically regulate NRTN production, muscarinic agonists have been shown to modulate the production of other neurotrophins, such as nerve growth factor (NGF) in gastric epithelial (*75*) and adipose (*76*) cells, to promote innervation, suggesting this as a potential mechanism by which CV acts in the salivary glands. Whether this is the case remains to be determined.

Given that a chronic proinflammatory response to radiation damage is a major contributor to human salivary gland dysfunction and degeneration, with irradiated human salivary glands exhibiting extensive lymphocytic infiltration (*77*), controlling this outcome is also required to enable robust tissue regeneration. We found that CV treatment reduced the proinflammatory state and instead promoted a pro-repair immune response in the salivary glands after radiation, an outcome consistent with a regenerative rather than degenerative response. The cholinergic system has previously been described as anti-inflammatory, with a growing number of studies reporting neuronal acetylcholine to attenuate the production of proinflammatory cytokines via α7 nicotinic receptors on macrophages, microglia, and astrocytes (*78*). However, the role of muscarinic receptors in the regulation of immune cell identity and function remains poorly understood. Although a number of previous studies primarily link muscarinic signaling in immune cells to proinflammatory outcomes, including the expansion of macrophages (*79*), more recent studies have suggested an anti-inflammatory role. In the murine small intestine, genetic deletion of *Chrm3* was associated with an up-regulation of proinflammatory T helper 1 (T_H1)/T_H17 cytokines in the absence of infection (*80*). Furthermore, upon infection with the nematode *Nippostrongylus brasiliensis*, $Chrm3^{-/-}$ mice were unable to mount the appropriate anti-inflammatory T_H2 responses required to efficiently clear the infection (*80*). This is significant because M1 (proinflammatory) macrophages promote T_H1 responses, which then suppress M2 (pro-reparatory) macrophage polarization, and vice versa, with M2 macrophages and T_H2 responses suppressing M1 macrophage polarization (*81*). Consistent with this outcome, we show that CV treatment, as opposed to ALG or saline, results in the specific expansion of the M2 subtype and reduces T cell infiltration, thus supporting muscarinic agonism as a mitigator of inflammation and a promoter of wound healing under radiation conditions. However, further studies are required to confirm that this is indeed the case.

Together, our muscarinic-based alginate treatment is able to produce a functional secretory tissue with preserved innervation after radiation exposure. Ultimately, this therapy is designed to be delivered directly within the gland space, with the periglandular delivery used here simply reflecting the limitation of the rodent model. However, the beneficial cellular changes that we observed at both the acinar cell and nerve levels, and the maintenance of saliva secretion itself, demonstrate that this is a promising treatment for the functional improvement in saliva output in those suffering from radiation-induced xerostomia.

MATERIALS AND METHODS

Animal studies

Adult female mice (6 to 7 weeks) from the C57BL/6 inbred strain (Harlan Laboratories) were used in all experiments. Mice were housed in the Association for Assessment and Accreditation of

Laboratory Care (AAALAC)-accredited University of California, San Francisco (UCSF) Parnassus campus Laboratory Animal Resource Center. Sample size was determined on the basis of previous studies (*3*, *10*) and a power analysis. All animals were given a unique ID number and hence were blinded to the researcher during analysis. Animals received either no radiation or a single 10-Gy dose, as described below. At the end of experiments, animals were euthanized using CO_2 at a flow of 2 liters/min followed by a cervical dislocation.

γ-Radiation of salivary glands

A group of mice was treated with a single 10-Gy dose of γ-radiation 14 days before treatment, as previously described (*10*, *82*). Animals were placed into the Shepherd Mark I Cesium Irradiator (JL Shepherd & Associates), with the body and cranial regions shielded from radiation using lead blocks. The lower head and neck regions of mice were exposed to radiation at a dose rate of 167 rad/min for 6 min for a total dose of 10 Gy, with the dose being calculated to the midline. A control group of mice was also anesthetized under the same conditions but did not undergo radiation treatment. Mice were allowed to completely recover following anesthesia, and their well-being was monitored for the first 48 hours. To ensure adequate food intake, all mice were given a soft diet ad libitum (clear H_2O). Mice were then sacrificed at 7, 14, 15, 17, 21, 70, or 93 days after radiation.

Oxidized ALG

Oxidized alginate was prepared by reacting sodium alginate (Protanal LF 20/40, alginate molecular weight = 197,000 Da, FMC Biopolymer #S18407) with sodium periodate (Sigma-Aldrich, catalog no. 311448) using a modification of a previously described method (*46*). Briefly, sodium alginate (10 g) was dissolved in ultrapure deionized water (diH_2O; 900 ml) overnight. Sodium periodate (0.22 g) was dissolved in 100 ml of diH_2O and added to alginate solution under stirring in the dark at room temperature (RT). After reacting for 24 hours, the reaction was stopped by addition of ethylene glycol (52 μl; Sigma-Aldrich). The alginate was purified by dialysis (molecular weight cutoff = 3500 Da, Spectrum Laboratories Inc.) against diH_2O for 3 days, treated with activated charcoal (5 g/liter; 50 to 200 mesh; Thermo Fisher Scientific, 05-690B) for 30 min, filtered (0.22-μm filter), and lyophilized. To determine oxidation efficiency, alginate was dissolved in deuterium oxide (5%, w/v) and placed in a nuclear magnetic resonance (NMR) tube. ^{13}C-NMR spectrum was recorded on a Bruker ADVANCE III 400-MHz NMR spectrometer (Bruker) using 3-(trimethylsilyl) propionic acid-d_4 sodium salt (0.05%, w/v) as an internal standard. Oxidation was determined from ^{13}H-NMR spectrum based on the ratio of the integrals for the carbons to the newly formed carbonyl carbons of aldehydes by oxidation of alginate (fig. S2B). Alginate was maintained at −20°C in a lyophilized form until ready to synthesize for injection. Immediately before in vivo delivery, lyophilized alginate (50 mg) was dissolved in Dulbecco′s modified Eagle′s medium (DMEM; 894.2 μl; Gibco, #11885084) containing CV (84.8 μl of 100 mM CV; Sigma-Aldrich, SML0007) or sterile ribonuclease-free water (84.8 μl; Invitrogen, #10977015). Alginate was then partially cross-linked ex vivo by mixing vigorously for 1 min with 100 μl of supersaturated calcium sulfate solution ($CaSO_4$; 210 mg/ml) using two syringes connected with a Luer-lock, and cross-linking is completed following in vivo injection.

CV release from ALGs

In vitro CV release from the ALGs was quantified by making 4 mm × 1 mm alginate + CV hydrogel disks containing 1.5 mg of CV each. Hydrogel disks were formed by injecting the partially cross-linked alginate + CV between two glass plates with a 1-mm spacer. Polymerization was completed by incubating at the fixture at RT for 30 min. Glass was removed, and then a 4-mm biopsy punch was used to create uniform disks. Disks were transferred to a 0.4-μm transwell (Millicell, #MCHT12H48) in a 12-well plate containing 3.2 ml of DMEM and incubated at 37°C with slow continuous agitation (100 rpm). Sample medium (3 ml of DMEM) was collected and fully replenished at 4 hours and 1, 2, 3, 4, 5, and 7 days. Sample medium was stored at −20°C, and CV was quantified by mass spectroscopy (Shimadzu Prominence LC-20ADXR interfaced to a 4500 QTrap mass spectrometer) using the Mass Spectroscopy Core Facility at the Zuckerberg San Francisco General Hospital under the direction of K. Lynch. T_0 (initial control) gels were dissolved in DMEM to establish the baseline of CV encapsulated in hydrogel.

Periglandular application of saline, CV, alginate, or alginate + CV 14 days after radiation exposure

In vivo delivery of saline, CV, alginate, or alginate + CV was achieved via subcutaneous injection superficial to both the sublingual and submandibular salivary glands without surgical exposure (as detailed below) 14 days after radiation-induced damage. Animals were anesthetized using isoflurane (2.5% induction, 1.5% maintenance), skin was cleaned with alternating iodine and alcohol washes, and 50 μl of saline, CV, alginate alone, or alginate + CV was administered by subcutaneous injection using a 25-gauge × $^5/_8$ needle placed at an angle of 45° to the tissue. The location of each injection was 0.5 cm to the left or to the right of the midline, between c2 and c5 vertebra. To ensure correct localization of the ALGs around the salivary gland, iohexol (MilliporeSigma, 74147), a radio-opaque contrast reagent, was encapsulated into the hydrogels at a concentration of 0.35 g/ml, and the Hologic Fluoroscan Premier Encore 60000 C-Arm Imaging System (45 kV, 0.031 mA) was used to visualize the material. In addition to a single dose of each treatment at 14 days after radiation, some mice that were treated initially with a single dose of saline or alginate + CV were subsequently injected with multiple doses of saline or CV (50 μl; Fig. 4) beginning at 38 days after radiation. A single dose of each treatment was administered once per week until 87 days after radiation. Saliva was collected (as described below) before mice were euthanized at the end of each experiment (n = 3 to 6). Sublingual and submandibular glands were then processed for immunofluorescent analysis, as described below.

Physiological saliva collection (gustatory stimulated)

Physiological saliva secretion was measured using gustatory stimulation (mornings at 9:00 a.m.), as previously published with some minor modifications (*39*). Briefly, a 7.5 cm × 10 cm filter paper (Bio-Rad, 1703932) was incubated in sodium citrate (73.6 mg/ml; Spectrum Chemical, S1250) solution for 15 min at RT on an orbital shaker and then dried overnight at RT. The filter paper was then cut into 30 mm × 2 mm strips, and the middle point was labeled on each strip. Individual strips were then placed in preweighed 1.5-ml microcentrifuge tubes. After mice were anesthetized by 2% inhaled isoflurane, a strip of filter paper was inserted into the oral cavity on top of the tongue until the maxillary incisors reached

the middle point of the strip. After 20 min, the strip was removed and placed in the original 1.5-ml microcentrifuge tube. The amount of saliva collected was determined by measuring the difference in weight of the microcentrifuge tube with filter paper before and after collection, using a precision scale (OHAUS Adventurer). For mice receiving single doses of each treatment, saliva was collected once per week from 35 to 63 days after radiation (Fig. 3). For mice receiving multiple doses of saline or CV (as well as their controls; Fig. 4), saliva was collected every 2 weeks from 35 to 91 days after radiation. Saliva was collected 4 days after injection to ensure that saliva output was not induced by remaining CV.

Maximum saliva collection (pilocarpine stimulated)

Maximum saliva output was measured at 14, 70, or 93 days after radiation, as described previously (*83*). Briefly, pilocarpine (68 ng/μl; Sigma-Aldrich, P0472) in saline (Aspen, AHI14208186) solution was freshly prepared before saliva collection. Mice were anesthetized by 2% inhaled isoflurane, pilocarpine (200 μl/30 g of body weight of 68 ng/μl) was intraperitoneally injected, and then animals were placed back in the anesthetizing chamber for 3 min. Preweighed cotton balls (Puritan, 806-WCL) were inserted into the mouths of the mice. After 5 min, one cotton ball was exchanged for another and left for another 5 min; in total, saliva was collected for 10 min using two cotton balls. These balls were placed back in the original 1.5-ml microcentrifuge tube, and the amount of saliva collected was determined by measuring the difference in weight of the cotton balls before and after collection, using a precision scale (OHAUS Adventurer).

Preparation of tissue samples for RNA-seq and immunofluorescent analyses

For RNA analysis, tissue was snap-frozen and stored at −80°C. For immunofluorescent analysis, tissue was either freshly frozen in optimal cutting temperature compound (OCT; Tissue-Tek) and stored at −80°C or immediately fixed with 4% paraformaldehyde (PFA) overnight at 4°C. Fixed samples were washed with phosphate-buffered saline (PBS), cryoprotected by immersion in 12.5 and 25% sucrose solution, then embedded in OCT, and stored at −80°C. Tissues were sectioned (12 μm) with a cryostat (Thermo Fisher Scientific) for immunofluorescence staining, as described below.

Bulk RNA-seq of salivary glands

RNA was isolated from four 50-μm tissue sections of non-IR or 7- or 14-day post-IR sublingual glands using the RNAqueous Micro Kit (Thermo Fisher Scientific, AM1931), and total RNAs were treated with deoxyribonuclease I (Thermo Fisher Scientific). RNA integrity and quantification were assessed using the RNA Nano 6000 Kit of the Bioanalyzer 2100 system (Agilent Technologies, CA). RNA-seq was performed by Novogene (https://en.novogene.com) using Illumina NovaSeq 6000 platform. Raw data (FASTQ) were processed through fastp. Paired-end clean reads were aligned to the reference genome using the Spliced Transcripts Alignment to a Reference (STAR) software (*84*). FeatureCounts was used to count the read numbers mapped to each gene (*85*). Differential expression analysis between two conditions was performed using DESeq2 R package (*24*). Genes with an adjusted P value of <0.05 were assigned as differentially expressed. GO of differentially expressed genes was analyzed using g:Profiler (*25*).

EdU delivery and detection

To quantify the rate of cell turnover, non-IR and IR animals were systemically injected with 0.9% saline containing 0.25 mg per 25 g of body weight of EdU (Thermo Fisher Scientific) that was followed by a 2-hour, 3-day, or 7-day chase (where "chase" is the waiting period after EdU injection) before mice were sacrificed. EdU detection was performed using the Click-iT EdU Imaging Kit (Thermo Fisher Scientific, C10086) according to the manufacturer's instruction. Briefly, fresh-frozen sections were fixed with 4% PFA for 15 min at RT followed by two washes with 3% bovine serum albumin (BSA) in PBS. Immediately after BSA washes, the sections were immersed in freshly prepared reaction cocktail (430 μl of 1× Click-iT reaction buffer + 20 μl of $CuSO_4$ + 1.2 μl of Alexa Fluor azide + 50 μl of reaction buffer additive, in proportion). After 30 min of incubation, sections were washed twice with 3% BSA in PBS. Images were obtained with an LSM900 confocal microscope.

Immunofluorescence studies

Tissue section immunofluorescence analysis was completed as described previously (*16*). In brief, fresh-frozen tissue was fixed with 4% PFA for 10 min, or prefixed tissue was defrosted for 5 min, followed by permeabilization with 0.5% Triton X-100 in PBS for 10 min at RT. Tissue sections were blocked for 2 hours at RT with 10% donkey serum (The Jackson Laboratory, ME), 5% BSA (Sigma-Aldrich), and MOM immunoglobulin G–blocking reagent if required (Vector Laboratories, CA) in 0.01% PBS–Tween 20. Salivary gland sections were incubated with the following primary antibodies overnight at 4°C: stem cell antibody goat anti-SOX2 (1:200; Neuromics, GT15098); epithelial cell antibody, rat anti–E-cadherin (1:400; Invitrogen, 13-1900); cell proliferation antibody, rabbit anti-pHH3 (1:200; Cell Signaling Technology, #9701); muscarinic M3 receptor (CHRM3) antibody, rabbit anti-CHRM3 (1:500; Research Diagnostics, AS-3741S); acinar antibodies rabbit anti-AQP5 (1:200; Millipore, AB3559) and anti-MUC10 (1:200; Abcore, AC21-2394); immune cell antibodies rat anti-CD68 (1:400; Bio-Rad, MCA1957), rabbit anti-CD3 (1:200; Abcam, ab5690), and rabbit anti-CD206/MMR (1:200; AF2535, R&D Systems); parasympathetic nerve/Schwann cell marker, goat anti-GFRα2 (1:200; R&D Systems, AF429); and VIP antibody anti-VIP (1:100; Abcam, ab124788). Antibodies were detected using Cy2-, Cy3-, or Cy5-conjugated secondary Fab fragment antibodies (1:300; The Jackson Laboratory), and nuclei were stained using Hoechst 33342 (1:1000; AnaSpec Inc.). Slides were mounted using Fluoromount-G (SouthernBiotech), and images were taken using an LSM900 confocal microscope. Image processing and quantification were performed using National Institutes of Health (NIH) ImageJ software or Imaris v9.6 (Bitplane). For image analysis, three to five fields of 250 μm × 250 μm × 12 μm (1-μm z sections) were imaged within different sections of the tissue.

Quantification of immunofluorescent images and specific cell populations

For each treatment group, tissues were sectioned (via cryostat) from the exterior to the interior of the gland. Every second tissue section was taken for immunostaining, with each section being x = 3.5 mm, y = 3 mm, and z = 12 μm in size. Imaging was performed on three to five fields of view measuring x = 250 μm, y = 250 μm, and z = 12 μm, with the z axis being composed of 1-μm sections consolidated into a 12-μm projection. Fields of view were selected at three distinct

locations across the tissue section (0.5 to 1 mm apart) and based on enrichment in acinar cells.

Acinar cells were identified on the basis of NKCC1 or AQP5 expression, proliferating cells were identified on the basis of EdU incorporation or pHH3 expression, and immune cells were identified on the basis of the T cell marker CD3 or the macrophage markers CD68 and CD206. Quantification of cells was achieved by applying the image processing software ImageJ (NIH) and manually counting cells. Acinar cell boundaries were determined by AQP5, NKCC1, or E-cadherin (CDH1) expression. The number of acinar cells was normalized to the total number of nuclei per section, and the number of proliferating acinar cells was normalized to the total acinar cell number per region. The number of immune cells was normalized to the total number of nuclei per section. Each quantification was performed on three to four sections per gland, from at least three animals.

Quantification of GFRa2$^+$ parasympathetic nerves and the neuropeptide VIP was achieved through analysis of 256 μm × 256 μm images within a 12 μm × 1 μm projection. Three separate regions of each gland that were enriched in acinar cells were imaged per animal (n = 3). Using the image analysis and visualization software Imaris v9.6 (Bitplane), which provides unbiased measurements of immunofluorescence, images were subjected to Gaussian filtering and background subtraction. Surface reconstructions were made with the "Surfaces" module. GFRa2$^+$ nerve fibers were manually traced with the "Filaments" module, "AutoPath" function. Mean volumes and filament diameters were exported from the statistics tab and analyzed in Microsoft Excel and GraphPad Prism. Filament diameters of <1.5 μm were based on control glands and on previous publications (*86*, *87*). VIP was measured with the "Spots" module, with a distance of less than 4.5 μm to the GFRa2$^+$ nerve fibers. Total GFRa2$^+$ nerve fibers and VIP counts were exported from the statistics tab and analyzed in Microsoft Excel and GraphPad Prism.

Statistical analyses

Statistical tests were performed using GraphPad Prism software v8. Data are plotted as individual data points with means ± SD. Groups with only two datasets were analyzed with a two-tailed unpaired Student's t test. For multiple comparisons, an ordinary one-way analysis of variance (ANOVA) was used to determine whether significant differences existed, followed by either a Tukey's post hoc comparisons test (for comparing means of multiple groups) or a Dunnett's test. Significance was assessed using P value cutoffs indicated as follows: $^*P < 0.05$, $^{**}P < 0.01$, $^{***}P < 0.001$, and $^{****}P < 0.0001$. Specific dataset analyses are described in the figure legends.

Study approval

All procedures were approved by the UCSF Institutional Animal Care and Use Committee and were adherent to the NIH *Guide for the Care and Use of Laboratory Animals*.

Supplementary Materials

This PDF file includes:
Figs. S1 to S4

Other Supplementary Material for this manuscript includes the following:
Data S1 to S3

View/request a protocol for this paper from *Bio-protocol*.

REFERENCES AND NOTES

1. O. M. Maria, N. Eliopoulos, T. Muanza, Radiation-induced oral mucositis. *Front. Oncol.* **7**, 89 (2017).
2. H. Lu, Q. Zhao, J. Guo, B. Zeng, X. Yu, D. Yu, W. Zhao, Direct radiation-induced effects on dental hard tissue. *Radiat. Oncol.* **14**, 5 (2019).
3. I. M. A. Lombaert, J. F. Brunsting, P. K. Wierenga, H. H. Kampinga, G. de Haan, R. P. Coppes, Cytokine treatment improves parenchymal and vascular damage of salivary glands after irradiation. *Clin. Cancer Res.* **14**, 7741–7750 (2008).
4. J. J. Sciubba, D. Goldenberg, Oral complications of radiotherapy. *Lancet Oncol.* **7**, 175–183 (2006).
5. K. J. Jasmer, K. E. Gilman, K. M. Forti, G. A. Weisman, K. H. Limesand, Radiation-induced salivary gland dysfunction: Mechanisms, therapeutics and future directions. *J. Clin. Med.* **9**, 4095 (2020).
6. R. L. Siegel, K. D. Miller, H. E. Fuchs, A. Jemal, Cancer statistics, 2022. *CA Cancer J. Clin.* **72**, 7–33 (2022).
7. S. B. Jensen, A. Vissink, K. H. Limesand, M. E. Reyland, Salivary gland hypofunction and xerostomia in head and neck radiation patients. *J. Natl. Cancer Inst. Monogr.* **2019**, lgz016 (2019).
8. D. S. Chang, F. D. Lasley, I. J. Das, M. S. Mendonca, J. R. Dynlacht, Normal tissue radiation responses, in *Basic Radiotherapy Physics and Biology* (Springer, 2014), pp. 265–275.
9. L. Barazzuol, R. P. Coppes, P. van Luijk, Prevention and treatment of radiotherapy-induced side effects. *Mol. Oncol.* **14**, 1538–1554 (2020).
10. E. Emmerson, A. J. May, L. Berthoin, N. Cruz-Pacheco, S. Nathan, A. J. Mattingly, J. L. Chang, W. R. Ryan, A. D. Tward, S. M. Knox, Salivary glands regenerate after radiation injury through SOX2-mediated secretory cell replacement. *EMBO Mol. Med.* **10**, e8051 (2018).
11. S. M. Knox, I. M. A. Lombaert, C. L. Haddox, S. R. Abrams, A. Cotrim, A. J. Wilson, M. P. Hoffman, Parasympathetic stimulation improves epithelial organ regeneration. *Nat. Commun.* **4**, 1494 (2013).
12. K. Abok, U. Brunk, B. Jung, J. Ericsson, Morphologic and histochemical studies on the differing radiosensitivity of ductular and acinar cells of the rat submandibular gland. *Virchow Arch. B Cell Pathol. Incl. Mol. Pathol.* **45**, 443–460 (1984).
13. A. C. O'Connell, R. S. Redman, R. L. Evans, I. S. Ambudkar, Radiation-induced progressive decrease in fluid secretion in rat submandibular glands is related to decreased acinar volume and not impaired calcium signaling. *Radiat. Res.* **151**, 150–158 (1999).
14. M. Muhvic-Urek, M. Bralic, S. Curic, S. Pezelj-Ribaric, J. Borcic, J. Tomac, Imbalance between apoptosis and proliferation causes late radiation damage of salivary gland in mouse. *Physiol. Res.* **55**, 89–95 (2006).
15. M. E. Luitje, A. K. Israel, M. A. Cummings, E. J. Giampoli, P. D. Allen, S. D. Newlands, C. E. Ovitt, Long-term maintenance of acinar cells in human submandibular glands after radiation therapy. *Int. J. Radiat. Oncol. Biol. Phys.* **109**, 1028–1039 (2021).
16. C. Zheng, A. P. Cotrim, A. Rowzee, W. Swaim, A. Sowers, J. B. Mitchell, B. J. Baum, Prevention of radiation-induced salivary hypofunction following hKGF gene delivery to murine submandibular glands. *Clin. Cancer Res.* **17**, 2842–2851 (2011).
17. O. Grundmann, G. C. Mitchell, K. H. Limesand, Sensitivity of salivary glands to radiation: From animal models to therapies. *J. Dent. Res.* **88**, 894–903 (2009).
18. A. Martinez Chibly, T. Nguyen, K. H. Limesand, Palliative care for salivary gland dysfunction highlights the need for regenerative therapies: A review on radiation and salivary gland stem cells. *J. Palliat. Care Med.* **4**, 1000180 (2014).
19. A. B. Houssay, A. A. Peronace, C. J. Perec, O. Rubinstein, Role of the chorda tympani in submaxillary hypertrophy by incisor amputation in the rat. *Acta Physiol. Lat. Am.* **12**, 153–166 (1962).
20. C. A. Schneyer, H. D. Hall, Amylase and electrolyte changes after postganglionic parasympathectomy of parotid gland. *Am. J. Physiol.* **207**, 308–312 (1964).
21. S. Zhang, Y. Su, G. Zheng, Y. Liang, G. Liao, Reinnervated nerves contribute to the secretion function and regeneration of denervated submandibular glands in rabbits. *Eur. J. Oral Sci.* **122**, 372–381 (2014).
22. N. Emmelin, C. Perec, Reinnervation of submaxillary glands after partial postganglionic denervation. *Q. J. Exp. Physiol. Cogn. Med. Sci.* **53**, 10–18 (1968).
23. B. U. Coskun, H. Savk, E. D. Cicek, T. Basak, M. Basak, B. Dadas, Histopathological and radiological investigations of the influence of botulinum toxin on the submandibular gland of the rat. *Eur. Arch. Otorhinolaryngol.* **264**, 783–787 (2007).

24. M. I. Love, W. Huber, S. Anders, Moderated estimation of fold change and dispersion for RNA-seq data with DESeq2. *Genome Biol.* **15**, 550 (2014).
25. J. Reimand, M. Kull, H. Peterson, J. Hansen, J. Vilo, G:Profiler-a web-based toolset for functional profiling of gene lists from large-scale experiments. *Nucleic Acids Res.* **35**, W193–W200 (2007).
26. T. Ban, G. R. Sato, T. Tamura, Regulation and role of the transcription factor IRF5 in innate immune responses and systemic lupus erythematosus. *Int. Immunol.* **30**, 529–536 (2018).
27. R. Colina, M. Costa-Mattioli, R. J. O. Dowling, M. Jaramillo, L. H. Tai, C. J. Breitbach, Y. Martineau, O. Larsson, L. Rong, Y. V. Svitkin, A. P. Makrigiannis, J. C. Bell, N. Sonenberg, Translational control of the innate immune response through IRF-7. *Nature* **452**, 323–328 (2008).
28. A. Mildner, J. Schönheit, A. Giladi, E. David, D. Lara-Astiaso, E. Lorenzo-Vivas, F. Paul, L. Chappell-Maor, J. Priller, A. Leutz, I. Amit, S. Jung, Genomic characterization of murine monocytes reveals C/EBPβ transcription factor dependence of Ly6C-cells. *Immunity* **46**, 849–862.e7 (2017).
29. M. M. Urek, M. Bralic, J. Tomac, J. Borcic, I. Uhac, I. Glazar, R. Antonic, S. Ferreri, Early and late effects of X-irradiation on submandibular gland: A morphological study in mice. *Arch. Med. Res.* **36**, 339–343 (2005).
30. Y. Wei, L. Yu, J. Bowen, M. A. Gorovsky, C. D. Allis, Phosphorylation of histone H3 is required for proper chromosome condensation and segregation. *Cell* **97**, 99–109 (1999).
31. M. H. Aure, S. F. Konieczny, C. E. Ovitt, Salivary gland homeostasis is maintained through acinar cell self-duplication. *Dev. Cell* **33**, 231–237 (2015).
32. J. R. Garrett, The proper role of nerves in salivary secretion: A review. *J. Dent. Res.* **66**, 387–397 (1987).
33. J. Drinjakovic, H. Jung, D. S. Campbell, L. Strochlic, A. Dwivedy, C. E. Holt, E3 ligase Nedd4 promotes axon branching by downregulating PTEN. *Neuron* **65**, 341–357 (2010).
34. K. Hsiao, H. Harony-Nicolas, J. D. Buxbaum, O. Bozdagi-Gunal, D. L. Benson, Cyfip1 regulates presynaptic activity during development. *J. Neurosci.* **36**, 1564–1576 (2016).
35. E. R. Graf, H. M. Heerssen, C. M. Wright, G. W. Davis, A. DiAntonio, Stathmin is required for stability of the drosophila neuromuscular junction. *J. Neurosci.* **31**, 15026–15034 (2011).
36. S. M. Knox, I. M. A. Lombaert, X. Reed, L. Vitale-Cross, J. S. Gutkind, M. P. Hoffman, Parasympathetic innervation maintains epithelial progenitor cells during salivary organogenesis. *Science* **329**, 1645–1647 (2010).
37. R. Matsuo, T. Yamamoto, K. Yoshitaka, T. Morimoto, Neural substrates for reflex salivation induced by taste, mechanical, and thermal stimulation of the oral region in decerebrate rats. *Jpn. J. Physiol.* **39**, 349–357 (1989).
38. R. M. Bradley, M. Kim, Reflex connections, in *The Role of the Nucleus of the Solitary Tract in Gustatory Processing* (CRC Press/Taylor & Francis, 2007).
39. M. Ogawa, M. Oshima, A. Imamura, Y. Sekine, K. Ishida, K. Yamashita, K. Nakajima, M. Hirayama, T. Tachikawa, T. Tsuji, Functional salivary gland regeneration by transplantation of a bioengineered organ germ. *Nat. Commun.* **4**, 2498 (2013).
40. M. Kamiya, T. Kawase, K. Hayama, M. Tsuchimochi, K. Okuda, H. Yoshie, X-ray-induced damage to the submandibular salivary glands in mice: An analysis of strain-specific responses. *Biores. Open Access* **4**, 307–318 (2015).
41. R. P. Coppes, A. Meter, S. P. Latumalea, A. F. Roffel, H. H. Kampinga, Defects in muscarinic receptor-coupled signal transduction in isolated parotid gland cells after in vivo irradiation: Evidence for a non-DNA target of radiation. *Br. J. Cancer* **92**, 539–546 (2005).
42. D. M. Hariyadi, N. Islam, Current status of alginate in drug delivery. *Adv. Pharm. Sci.* **2020**, 8886095 (2020).
43. L. Hu, C. Sun, A. Song, D. Chang, X. Zheng, Y. Gao, T. Jiang, S. Wang, Alginate encapsulated mesoporous silica nanospheres as a sustained drug delivery system for the poorly water-soluble drug indomethacin. *Asian J. Pharm. Sci.* **9**, 183–190 (2014).
44. J. A. R. Barros, L. D. R. de Melo, R. A. R. da Silva, M. P. Ferraz, J. C. V. d. R. Azeredo, V. M. d. C. Pinheiro, B. J. A. Colaço, M. H. R. Fernandes, P. d. S. Gomes, F. J. Monteiro, Encapsulated bacteriophages in alginate-nanohydroxyapatite hydrogel as a novel delivery system to prevent orthopedic implant-associated infections. *Nanomedicine* **24**, 102145 (2020).
45. S. Cohen, E. Lobel, A. Trevgoda, Y. Peled, A novel in situ-forming ophthalmic drug delivery system from alginates undergoing gelation in the eye. *J. Control. Release* **44**, 201–208 (1997).
46. O. Jeon, J.-Y. Shin, R. Marks, M. Hopkins, T.-H. Kim, H.-H. Park, E. Alsberg, Highly elastic and tough interpenetrating polymer network-structured hybrid hydrogels for cyclic mechanical loading-enhanced tissue engineering. *Chem. Mater.* **29**, 8425–8432 (2017).
47. K. Hosoi, C. Yao, T. Hasegawa, H. Yoshimura, T. Akamatsu, Dynamics of salivary gland AQP5 under normal and pathologic conditions. *Int. J. Mol. Sci.* **21**, 1182 (2020).
48. L. Stephens, G. King, L. Peters, K. Ang, T. Schultheiss, J. Jardine, Acute and late radiation injury in rhesus monkey parotid glands. Evidence of interphase cell death. *Am. J. Pathol.* **124**, 469–478 (1986).
49. G. B. Proctor, G. H. Carpenter, Regulation of salivary gland function by autonomic nerves. *Auton. Neurosci.* **133**, 3–18 (2007).
50. L. Luo, D. D. M. O'Leary, Axon retraction and degeneration in development and disease. *Annu. Rev. Neurosci.* **28**, 127–156 (2005).
51. M. Matsui, D. Motomura, H. Karasawa, T. Fujikawa, J. Jiang, Y. Komiya, S. I. Takahashi, M. M. Taketo, Multiple functional defects in peripheral autonomic organs in mice lacking muscarinic acetylcholine receptor gene for the M3 subtype. *Proc. Natl. Acad. Sci. U.S.A.* **97**, 9579–9584 (2000).
52. L. V. Borovikova, S. Ivanova, M. Zhang, H. Yang, G. I. Botchkina, L. R. Watkins, H. Wang, N. Abumrad, J. W. Eaton, K. J. Tracey, Vagus nerve stimulation attenuates the systemic inflammatory response to endotoxin. *Nature* **405**, 458–462 (2000).
53. M. Rath, I. Müller, P. Kropf, E. I. Closs, M. Munder, Metabolism via arginase or nitric oxide synthase: Two competing arginine pathways in macrophages. *Front. Immunol.* **5**, 532 (2014).
54. K. E. Gilman, J. M. Camden, R. R. Klein, Q. Zhang, G. A. Weisman, K. H. Limesand, P2X7 receptor deletion suppresses γ-radiation-induced hyposalivation. *Am. J. Physiol. Regul. Integr. Comp. Physiol.* **316**, R687–R696 (2019).
55. J. Ekstrom, B. Mansson, G. Tobin, Vasoactive intestinal peptide evoked secretion of fluid and protein from rat salivary glands and the development of supersensitivity. *Acta Physiol. Scand.* **119**, 169–175 (1983).
56. D. Alterio, G. Marvaso, A. Ferrari, S. Volpe, R. Orecchia, B. A. Jereczek-Fossa, Modern radiotherapy for head and neck cancer. *Semin. Oncol.* **46**, 233–245 (2019).
57. Y. Shwartz, M. Gonzalez-Celeiro, C.-L. Chen, H. A. Pasolli, S.-H. Sheu, S. M.-Y. Fan, F. Shamsi, S. Assaad, E. T.-Y. Lin, B. Zhang, P.-C. Tsai, M. He, Y.-H. Tseng, S.-J. Lin, Y.-C. Hsu, Cell types promoting goosebumps form a niche to regulate hair follicle stem cells. *Cell* **182**, 578–593.e19 (2020).
58. X. Gao, D. Zhang, C. Xu, H. Li, K. M. Caron, P. S. Frenette, Nociceptive nerves regulate haematopoietic stem cell mobilization. *Nature* **589**, 591–596 (2021).
59. S. M. Wie, T. S. Adwan, J. DeGregori, S. M. Anderson, M. E. Reyland, Inhibiting tyrosine phosphorylation of protein kinase Cδ (PKCδ) protects the salivary gland from radiation damage. *J. Biol. Chem.* **289**, 10900–10908 (2014).
60. Y. Marmary, R. Adar, S. Gaska, A. Wygoda, A. Maly, J. Cohen, R. Eliashar, L. Mizrachi, C. Orfaig-Geva, B. J. Baum, S. Rose-John, E. Galun, J. H. Axelrod, Radiation-induced loss of salivary gland function is driven by cellular senescence and prevented by IL6 modulation. *Cancer Res.* **76**, 1170–1180 (2016).
61. S. Pringle, M. Maimets, M. van der Zwaag, M. A. Stokman, D. van Gosliga, E. Zwart, M. J. H. Witjes, G. de Haan, R. van Os, R. P. Coppes, Human salivary gland stem cells functionally restore radiation damaged salivary glands. *Stem Cells* **34**, 640–652 (2016).
62. L. S. Y. Nanduri, M. Maimets, S. A. Pringle, M. V. D. Zwaag, R. P. V. Os, R. P. Coppes, Regeneration of irradiated salivary glands with stem cell marker expressing cells. *Radiother. Oncol.* **99**, 367–372 (2011).
63. X. Peng, Y. Wu, U. Brouwer, T. van Vliet, B. Wang, M. Demaria, L. Barazzuol, R. P. Coppes, Cellular senescence contributes to radiation-induced hyposalivation by affecting the stem/progenitor cell niche. *Cell Death Dis.* **11**, 854 (2020).
64. J. Yamamoto, J. Imai, T. Izumi, H. Takahashi, Y. Kawana, K. Takahashi, S. Kodama, K. Kaneko, J. Gao, K. Uno, S. Sawada, T. Asano, V. V. Kalinichenko, E. A. Susaki, M. Kanzaki, H. R. Ueda, Y. Ishigaki, T. Yamada, H. Katagiri, Neuronal signals regulate obesity induced β-cell proliferation by FoxM1 dependent mechanism. *Nat. Commun.* **8**, 1930 (2017).
65. J. Metzen, F. Bittinger, C. J. Kirkpatrick, H. Kilbinger, I. Wessler, Proliferative effect of acetylcholine on rat trachea epithelial cells is mediated by nicotinic receptors and muscarinic receptors of the M1-subtype. *Life Sci.* **72**, 2075–2080 (2003).
66. B. Peter, M. A. Van Waarde, A. Vissink, E. J.'s-Gravenmade, A. W. Konings, Radiation-induced cell proliferation in the parotid and submandibular glands of the rat. *Radiat. Res.* **140**, 257–265 (1994).
67. P. L. Weng, M. H. Aure, T. Maruyama, C. E. Ovitt, Limited regeneration of adult salivary glands after severe injury involves cellular plasticity. *Cell Rep.* **24**, 1464–1470.e3 (2018).
68. S. J. Keely, J. M. Uribe, K. E. Barrett, Carbachol stimulates transactivation of epidermal growth factor receptor and mitogen-activated protein kinase in T_{84} cells: Implications for carbachol-stimulated chloride secretion. *J. Biol. Chem.* **273**, 27111–27117 (1998).
69. R. O. Messing, A. M. Stevens, E. Kiyasu, A. B. Sneade, Nicotinic and muscarinic agonists stimulate rapid protein kinase C translocation in PC12 cells. *J. Neurosci.* **9**, 507–512 (1989).
70. B. E. Slack, J. K. Blusztajn, Differential regulation of mTOR-dependent S6 phosphorylation by muscarinic acetylcholine receptor subtypes. *J. Cell. Biochem.* **104**, 1818–1831 (2008).
71. A. A. V. Peronace, T. A. Davison, A. B. Houssay, C. J. Perec, Alterations in submandibular and retrolingual glands following parasympathetic denervation in rats. *Anat. Rec.* **150**, 25–33 (1964).
72. J. H. Kang, B. K. Kim, B. I. Park, H. J. Kim, H. M. Ko, S. Y. Ynag, M. S. Kim, J. Y. Jung, W. J. Kim, W. M. Oh, S. H. Kim, J. H. Kim, Parasympathectomy induces morphological changes and

alters gene-expression profiles in the rat submandibular gland. *Arch. Oral Biol.* **55**, 7–14 (2010).

73. U. Pirvola, U. Arumae, M. Moshnyakov, J. Palgi, M. Saarma, J. Ylikoski, Coordinated expression and function of neurotrophins and their receptors in the rat inner ear during target innervation. *Hear. Res.* **75**, 131–144 (1994).
74. J. N. A. Ferreira, C. Zheng, I. M. A. Lombaert, C. M. Goldsmith, A. P. Cotrim, J. M. Symonds, V. N. Patel, M. P. Hoffman, Neurturin gene therapy protects parasympathetic function to prevent irradiation-induced murine salivary gland hypofunction. *Mol. Ther. Methods Clin. Dev.* **9**, 172–180 (2018).
75. Y. Hayakawa, K. Sakitani, M. Konishi, S. Asfaha, Z. Jiang, T. Tanaka, Z. A. Dubeykovskaya, X. Chen, A. M. Urbanska, K. Nagar, C. B. Westphalen, M. Quante, C. Lin, M. D. Gershon, A. Hara, D. Chen, D. L. Worthley, K. Koike, T. C. Wang, Nerve growth factor promotes gastric tumorigenesis through aberrant cholinergic signaling. *Cancer Cell* **31**, 21–34 (2017).
76. R. Piovesana, A. Faroni, M. Taggi, A. Matera, M. Soligo, R. Canipari, L. Manni, A. J. Reid, A. M. Tata, Muscarinic receptors modulate nerve growth factor production in rat Schwann-like adipose-derived stem cells and in Schwann cells. *Sci. Rep.* **10**, 7159 (2020).
77. A. Teymoortash, N. Simolka, C. Schrader, M. Tiemann, J. A. Werner, Lymphocyte subsets in irradiation-induced sialadenitis of the submandibular gland. *Histopathology* **47**, 493–500 (2005).
78. F. Mantelli, M. Massaro-Giordano, I. Macchi, A. Lambiase, S. Bonini, The cellular mechanisms of dry eye: From pathogenesis to treatment. *J. Cell. Physiol.* **228**, 2253–2256 (2013).
79. E. de la Torre, A. M. Genaro, M. L. Ribeiro, R. Pagotto, O. P. Pignataro, M. E. Sales, Proliferative actions of muscarinic receptors expressed in macrophages derived from normal and tumor bearing mice. *Biochim. Biophys. Acta* **1782**, 82–89 (2008).
80. L. P. Mclean, A. Smith, L. Cheung, J. J. Urban, R. Sun, V. Grinchuk, N. Desai, A. Zhao, J. P. Raufman, T. Shea-Donohue, Type 3 muscarinic receptors contribute to intestinal mucosal homeostasis and clearance of *Nippostrongylus brasiliensis* through induction of T_H2 cytokines. *Am. J. Physiol. Gastrointest. Liver Physiol.* **311**, G130–G141 (2016).
81. C. D. Mills, M1 and M2 macrophages: Oracles of health and disease. *Crit. Rev. Immunol.* **32**, 463–488 (2012).
82. A. J. May, N. Cruz-Pacheco, E. Emmerson, E. A. Gaylord, K. Seidel, S. Nathan, M. O. Muench, O. Klein, S. M. Knox, Diverse progenitor cells preserve salivary gland ductal architecture after radiation-induced damage. *Development* **145**, dev166363 (2018).
83. J. J. Varghese, I. L. Schmale, M. E. Hansen, S. D. Newlands, D. S. W. Benoit, C. E. Ovitt, Murine salivary functional assessment via pilocarpine stimulation following fractionated radiation. *J. Vis. Exp.* **135**, 57522 (2018).
84. A. Dobin, C. A. Davis, F. Schlesinger, J. Drenkow, C. Zaleski, S. Jha, P. Batut, M. Chaisson, T. R. Gingeras, STAR: Ultrafast universal RNA-seq aligner. *Bioinformatics* **29**, 15–21 (2013).
85. A. Mortazavi, B. A. Williams, K. McCue, L. Schaeffer, B. Wold, Mapping and quantifying mammalian transcriptomes by RNA-Seq. *Nat. Methods* **5**, 621–628 (2008).
86. T. FitzGibbon, Z. Nestorovski, Human intraretinal myelination: Axon diameters and axon/myelin thickness ratios. *Indian J. Ophthalmol.* **61**, 567–575 (2013).
87. E. F. Hauck, M. Schwefer, W. Wittkowski, H. W. Bothe, Measurements and mapping of 282,420 nerve fibers in the S1-5 nerve roots. *J. Neurosurg. Spine* **11**, 255–263 (2009).

Acknowledgments: We thank L. Selleri, J. Bush, and O. Klein for contributions to the manuscript. **Funding:** This work was supported by the National Institute of Dental and Craniofacial Research (NIDCR; 1R35DE028255), NIDCR C-DOCTOR (U24DE026914), and Tobacco Related Disease Research Program (TRDRP; 588359). **Author contributions:** Conceptualization: J.L., S.S., L.B., A.J.M., O.J., E.A., C.S.B., and S.M.K. Methodology: J.L., S.S., L.B., A.J.M., S.M., E.A.G., H.S., N.C.P., J.C.C., E.A., C.S.B., and S.M.K. Investigation: J.L., S.S., L.B., A.J.M., S.M., H.S., E.A.G., N.C.P., J.C.C., E.A., C.S.B., and S.M.K. Formal analysis: J.L., S.S., L.B., S.M., E.A.G., N.C.P., and C.S.B. Visualization: J.L., S.S., L.B., C.S.B., and S.M.K. Data curation: J.L., S.S., L.B., E.A., C.S.B., and S.M.K. Providing reagents: E.A. and O.J. Project administration: S.M.K. Funding acquisition: C.S.B. and S.M.K. Supervision: S.M.K. Writing—original draft: J.L., S.S., L.B., C.S.B., and S.M.K. Writing—review and editing: J.L., S.S., L.B., A.J.M., E.A.G., H.S., S.M., O.J., E.A., I.M.A.L., C.S.B., and S.M.K. **Competing interests:** S.M.K., C.S.B., E.A., and O.J. are inventors on a patent related to this work filed by UCSF (no. 17/312196, filed on 10 December 2019, published on 24 February 2022). The authors declare no other competing interests. **Data and materials availability:** All data needed to evaluate the conclusions in the paper are present in the paper and/or the Supplementary Materials. RNA-seq data have been deposited in the Gene Expression Omnibus database (https://ncbi.nlm.nih.gov/geo) under the accession no. GSE209931. The alginate can be provided by E.A. pending mutual agreement to collaborate, scientific review, and a completed material transfer agreement. Requests for the alginate should be submitted to E.A. (ealsberg@uic.edu).

Submitted 9 May 2022
Accepted 5 November 2022
Published 21 December 2022
10.1126/sciadv.adc8753